Petroleum Science 19 (2022) 2549–2571

Contents lists available at ScienceDirect

Petroleum Science

journal homepage: www.keaipublishing.com/en/journals/petroleum-science

Original Paper

Prediction of multiscale laminae structure and reservoir quality in fine-grained sedimentary rocks: The Permian Lucaogou Formation in Jimusar Sag, Junggar Basin

Xiao-Jiao Pang [a, b, *], Gui-Wen Wang [a, b, **], Li-Chun Kuang [c], Jin Lai [a, b], Yang Gao [d], Yi-Di Zhao [a, b], Hong-Bin Li [a, b], Song Wang [a, b], Meng Bao [a, b], Shi-Chen Liu [a, b], Bing-Chang Liu [a, b]

[a] State Key Laboratory of Petroleum Resources and Prospecting, China University of Petroleum (Beijing), Beijing, 102249, China
[b] College of Geosciences, China University of Petroleum (Beijing), Beijing, 102249, China
[c] Technology Administration Department, PetroChina Company Limited, Beijing, 100007, China
[d] Research Institute of Exploration and Development, Xinjiang Oilfield Company, PetroChina, Karamay, Xinjiang, 834000, China

ARTICLE INFO

Article history:
Received 5 January 2022
Received in revised form
15 May 2022
Accepted 5 August 2022
Available online 10 August 2022

Edited by Teng Zhu and Jie Hao

Keywords:
Fine-grained sedimentary rocks
Mineral composition
Multiscale laminae structure
Reservoir quality
Image logs
Lucaogou formation

ABSTRACT

Fine-grained sedimentary rocks have become a research focus as important reservoirs and source rocks for tight and shale oil and gas. Laminae development determines the accumulation and production of tight and shale oil and gas in fine-grained rocks. However, due to the resolution limit of conventional logs, it is challenging to recognize the features of centimeter-scale laminae. To close this gap, complementary studies, including core observation, thin section, X-ray diffraction (XRD), conventional log analysis, and slabs of image logs, were conducted to unravel the centimeter-scale laminae. The laminae recognition models were built using well logs. The fine-grained rocks can be divided into laminated rocks (lamina thickness of <0.01 m), layered rocks (0.01–0.1 m), and massive rocks (no layer or layer spacing of >0.1 m) according to the laminae scale from core observations. According to the mineral superposition assemblages from thin-section observations, the laminated rocks can be further divided into binary, ternary, and multiple structures. The typical mineral components, slabs, and T_2 spectrum distributions of various lamina types are unraveled. The core can identify the centimeter–millimeter-scale laminae, and the thin section can identify the millimeter–micrometer-scale laminae. Furthermore, they can detect mineral types and their superposition sequence. Conventional logs can identify the meter-scale layers, whereas image logs and related slabs can identify the laminae variations at millimeter–centimeter scales. Therefore, the slab of image logs combined with thin sections can identify laminae assemblage characteristics, including the thickness and vertical assemblage. The identification and classification of lamina structure of various scales on a single well can be predicted using conventional logs, image logs, and slabs combined with thin sections. The layered rocks have better reservoir quality and oil-bearing potential than the massive and laminated rocks. The laminated rocks' binary lamina is better than the ternary and multiple layers due to the high content of felsic minerals. The abovementioned results build the prediction model for multiscale laminae structure using well logs, helping sweet spots prediction in the Permian Lucaogou Formation in the Jimusar Sag and fine-grained sedimentary rocks worldwide.

1. Introduction

With the development of unconventional oil and gas exploration worldwide, fine-grained sedimentary rocks have gradually become a research focus as crucial reservoirs and source rocks for tight and shale oil and gas (Curtis, 2002; Hill et al., 2007; Loucks

* Corresponding author. China University of Petroleum (Beijing), 18 Fuxue Road, Changping, Beijing, 102249, China.
** Corresponding author. China University of Petroleum (Beijing), 18 Fuxue Road, Changping, Beijing, 102249, China.
E-mail addresses: xiaojiaopang0829@163.com (X.-J. Pang), wanggw@cup.edu.cn (G.-W. Wang).

https://doi.org/10.1016/j.petsci.2022.08.001

et al., 2009; Lai et al., 2015; Liu et al., 2020; Altawati et al., 2021; Li et al., 2021). Fine-grained sedimentary rocks are fine-grained sediments with particle sizes less than 0.0625 mm, are widely distributed globally (Liu et al., 2019b), and account for approximately two-thirds of the sedimentary rocks (Krumbein, 1947; Schieber, 1991; Saidian and Prasad, 2015; Liu et al., 2019b). Fine-grained rocks contain huge oil and gas resources in China, showing a broad prospect for tight and shale oil and gas exploration (Liu et al. 2018, 2019a, 2020, 2022b). Fine-grained sedimentary rocks are the source rocks of conventional hydrocarbon and unconventional oil and gas (tight oil and gas, shale oil and gas) reservoirs. Therefore, studying fine-grained sedimentary rocks has theoretical and practical significance (Zou et al., 2012; Chen et al., 2017; Wu et al., 2019; Li et al., 2020; Altawati et al., 2021). Due to the complexity and high grade of heterogeneity, detailed integration between geological and petrophysical studies are recommended to characterize the multiscale, highly heterogeneous layered rocks (Nabawy and El Sharawy, 2015; El Sharawy and Nabawy, 2016; Abuamarah et al., 2019; Nabawy et al., 2020).

Sedimentary laminae are the basic components of fine-grained sedimentary rocks, and most fine-grained sedimentary rocks contain laminae of micrometer–meter scales (Anderson, 1996; Yawar and Schieber, 2017; Ma et al., 2019; Zhao et al., 2019). Multiscale laminae structure occurs in fine-grained sedimentary rocks, and the features of laminae from macro- (meter scale) to micro-scales (millimeter to micrometer scales) can be obtained through various observation methods (Chen et al., 2017; Li et al. 2018, 2020). The vertical superposition of different rock types (lithology) within

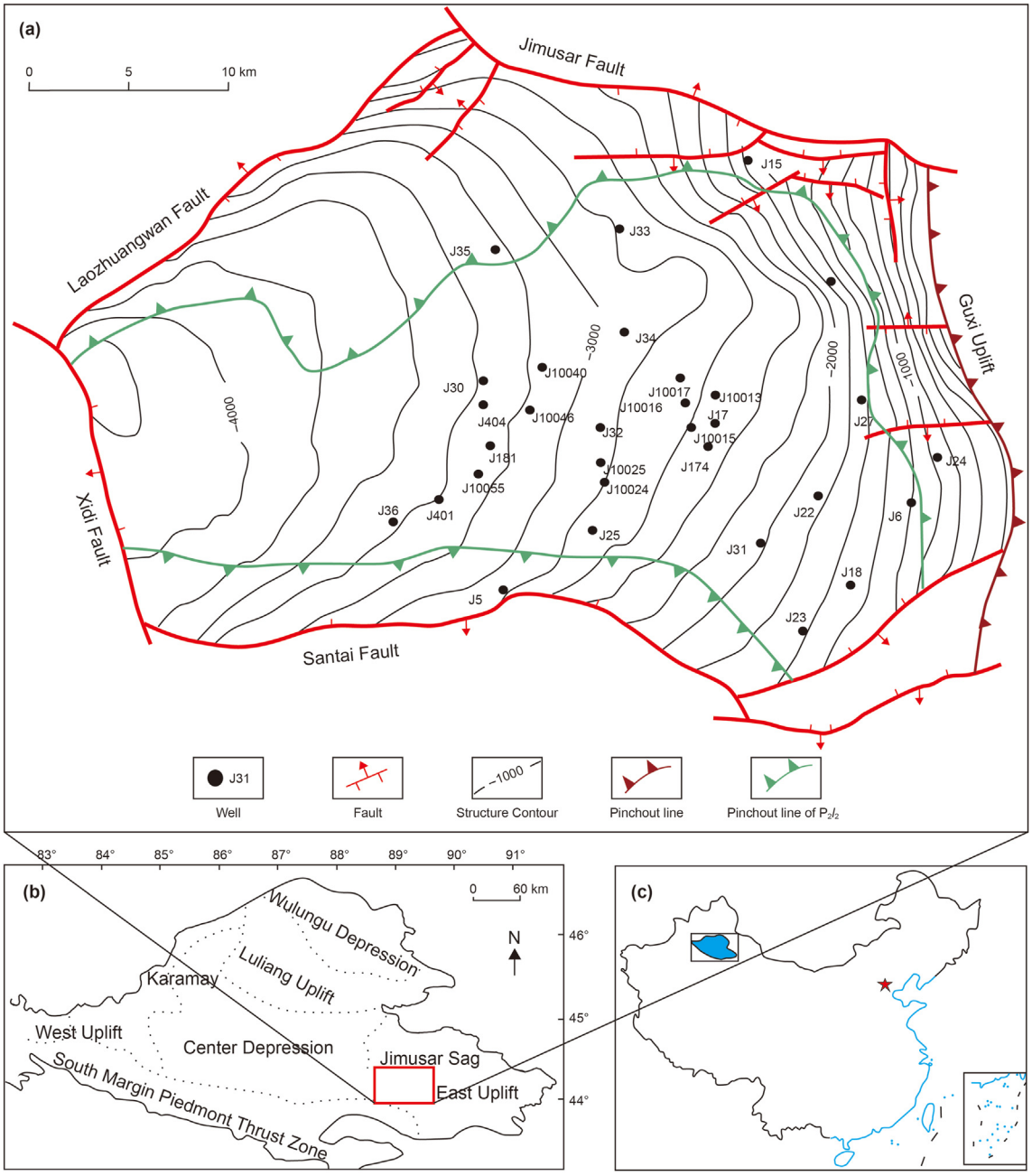

Fig. 1. (a) Structure characteristic map and well targeting Lucaogou Formation in the Jimusar Sag and location map of the Jimusar Sag in Junggar Basin (b) in China (c) (Kuang et al., 2012; Xi et al., 2015; Ma et al., 2020).

the range of meter–decimeter-scale lamina can be observed through outcrops and conventional well log data (Chen et al., 2017; Li et al., 2020). The millimeter–centimeter-scale laminated rocks formed by different mineral compositions in various superimposed ways on the centimeter-scale can be obtained from core observations (Chen et al., 2017; Li et al., 2020). Thin-section observation and scanning electron microscopy can obtain the millimeter–micrometer-scale laminated rocks formed by a mineral layer-superimposed sequence. Millimeter–micrometer-scale laminated rocks comprise binary (superimposition of two minerals), ternary (superimposition of three minerals), or multiple (superimposition of more than three minerals) laminae on the micron scale. The meter–centimeter lamina structure reflects the lithology variation, whereas the millimeter–micrometer lamina structure reflects the cyclicity changes of various mineral components (Rickman et al., 2008; Aplin and Macquaker, 2011; Chen et al., 2017; Li et al., 2020).

The lamina structure., i.e., the lamina scale and the superimposed sequence of mineral layers, determines the reservoir quality and oil-bearing properties in fine-grained sedimentary rocks (Li et al. 2018, 2020; Xi et al., 2020). Overall, the more developed the laminae in shales, the better the physical properties (Davies et al., 1991; Chen et al., 2017; Wang et al., 2019; Bai et al., 2022). The laminae also determine the crude oil occurrence and oil mobility (Tang et al., 2019; Zhao et al., 2019; Liu et al., 2021; Feng et al., 2021; Sun et al., 2022). Many geological factors control the laminae in fine-grained sedimentary rocks, and the multiscale laminae structure ranges from meter-scale lithology changes. The millimeter–micrometer-scale of mineral superimposition patterns is complex (Yuan et al., 2015; Liu et al., 2019b; Cai et al., 2022). Therefore, it is urgent to investigate the controlling relationships between the macroscopic physical properties of the reservoir and the multiscale laminae structure and mineral superposition sequences.

There are no comprehensive logging recognition methods for the multiscale laminae structure and the related reservoir quality it controls. Additionally, the laminae vary from meter to millimeter–micrometer scales, making it challenging to evaluate the lamina structure via well logs. This study uses core, thin section, conventional logs, image logs, and image log-derived slabs to unravel the multiscale laminae structure in the fine-grained sedimentary rocks of the Lucaogou Formation in the Jimusar Sag, Junggar Basin. The classification and logging characterization of various scale lamina structures and mineral superposition assemblages in fine-grained

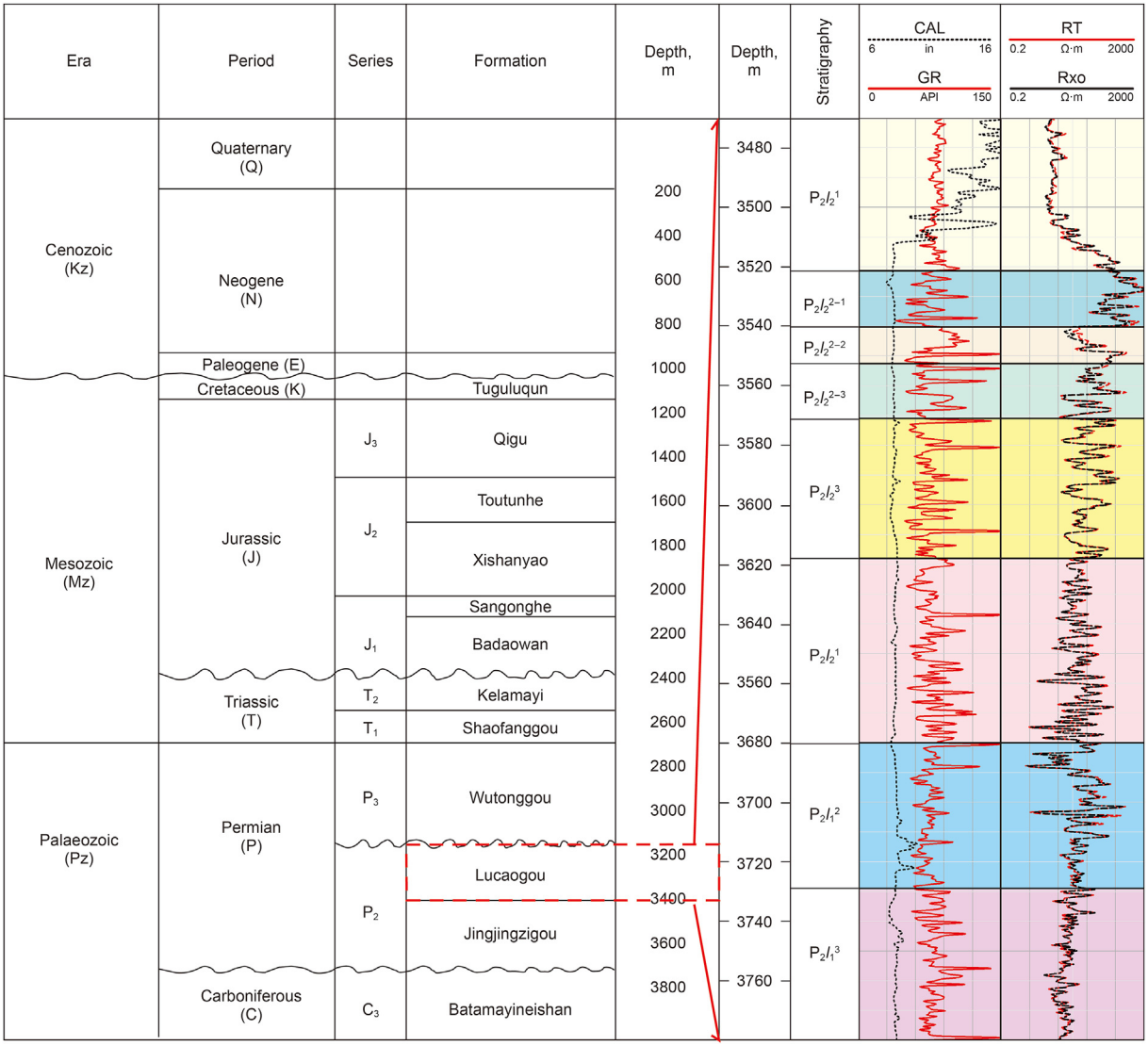

Fig. 2. Stratigraphic columns of the Permian Lucaogou Formation in Jimusar Sag, Junggar Basin (Modified after Cao et al., 2016).

sedimentary rocks are realized using core, thin sections, image logs, and slabs. The recognition methods of lamina structure ranging from the macroscopic lithology variations to microscopic mineral compositions are built using well logs. Furthermore, the vertical distribution of lamina structure and the related reservoir quality are unraveled. The research results provide insights into the lamina structure in fine-grained sedimentary rocks and predict the high-quality reservoirs in shale/tight oil play.

2. Geological settings

The Junggar Basin is a crucial petroliferous basin in Western China (Fig. 1) (Cao et al. 2016, 2020; Yang et al., 2019; Wang et al., 2020; Lin et al., 2021). The Jimusar Sag is in the southeast of the Junggar Basin, surrounded by several faults and highlands with obvious boundary features surrounded by the Qitai uplift, Santai uplift, Fukang fault zone, and Shaqi uplift, and the area is approximately 1,278 km^2 (Kuang et al., 2014; Zhao et al., 2014; Zhang et al., 2019; Ma et al., 2020) (Fig. 1a). The Jimusar Sag has experienced multiple stages of tectonic subsidence and uplift (Qiu et al., 2016; Cao et al., 2017; Wu et al., 2019). The Permian strata in the Jimusar Sag can be divided into the Jiangjunmiao Group (P_2j), Lucaogou Group (P_2l), and Wutonggou Group (P_2w) from the bottom to the top during the Hercynian tectonic episode with contemporaneous rifting and volcanic activities (Allen and ENGÖR, 1995; Xiao et al., 2008; Qi et al., 2013; Ma et al., 2020). The Lucaogou Formation, conformably overlying the Jiangjunmiao Formation and unconformably underlying the Wutonggou Formation, contains abundant shale oil resources, distributed throughout the sag with a thickness from 200 m to 350 m and covering 806 km^2 (Kuang et al., 2012; Xi et al., 2015; Zhang et al., 2019; Lin et al., 2021). The Lucaogou Formation is characterized by self-sourced, self-reservoir, and near-source hydrocarbon accumulation. The main exploration area's stratigraphy dip is moderately gentle with a structural dip angle from 3° to 5° (He et al., 2013; Zhao et al., 2014; Lu et al., 2015; Lai et al., 2022a). In the

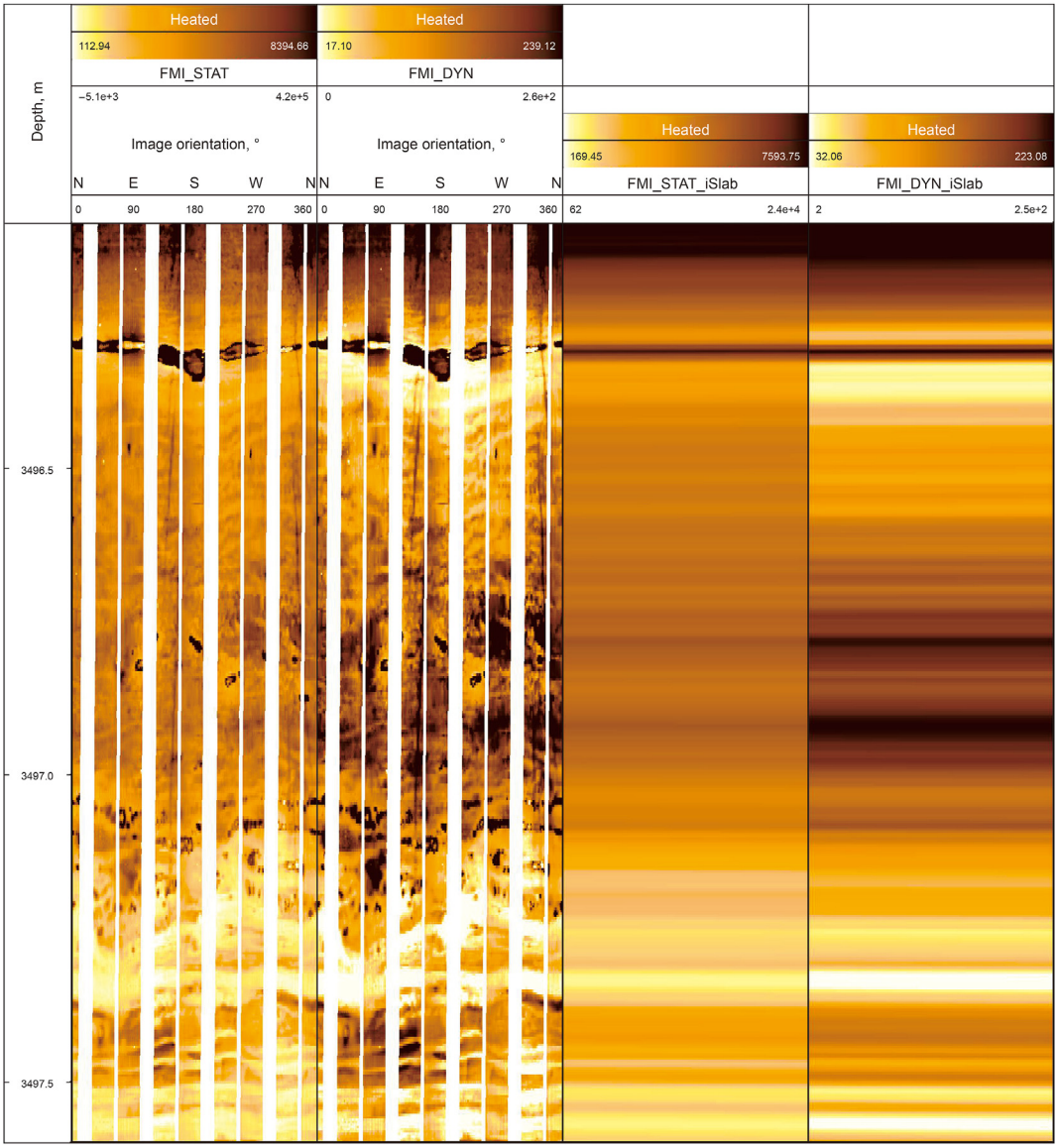

Fig. 3. Slab derived from image logs in fine-grained sedimentary rocks in the Permian Lucaogou Formation in the Jimusar Sag (J10016). The first track shows the depth, and the second is static image logs, and the third track is the dynamic image logs, the fourth and fifth tracks are the static and dynamic slabs. The slabs show more bedding characteristics than the image logs.

Yanshan movement, the tectonic activity was intense (Wang et al., 2020). During the Indosinian movement in the Late Jurassic, the Guxi uplift rose significantly, resulting in the erosion of the Permian and Triassic strata (Yang et al., 2019).

The entire Lucaogou Formation is deposited in a saline shore-lake environment (Gao et al., 2016; Zhang et al., 2017). The Permian Lucaogou Formation's source rocks went through the oil generation window after the Late Triassic and experienced two oil generation and expulsion stages during the Jurassic and Cretaceous (Qiu et al., 2016). The Lucaogou Formation can be divided into the lower part (P_2l_1) and the upper part (P_2l_2) from the bottom to the top according to the maximum flooding surface and lithological associations (Kuang et al., 2012; Pang et al., 2022). It can be further subdivided into six sandbody associations ($P_2l_2^1$, $P_2l_2^2$, $P_2l_2^3$, $P_2l_1^1$, $P_2l_1^2$, and $P_2l_1^3$) (Fig. 2). Two sweet spot sets (high-quality reservoirs) have been found vertically in the $P_2l_2^2$ and $P_2l_1^2$ (Liu et al., 2020). Many recently drilled wells had obtained commercial oil flows, and the oil test results reveal promising oil exploration potential.

3. Materials and methods

Core plug samples of fine-grained sedimentary rock were obtained from Wells J10016, J10022, and J10025 in the Middle Permian Lucaogou Formation in the Jimusar Sag (Fig. 1). This study used 32 core plug samples to conduct experiments for obtaining the geological properties. These experiments included thin sections and X-ray diffraction (XRD). The core plugs were cut into 30 μm thickness and then were examined using Leica optical microscopy under plane-polarized light (PPL) and cross-polarized light (XPL). Before the thin section preparation, blue or red fluorescent epoxy was impregnated into rocks to highlight the pores. Thin sections were also stained with mixed Alizarin Red and potassium ferricyanide solution to differentiate Ferroan–calcite from Ferroan–dolomite calcite. The mineralogy was based on XRD, and the data of these tests are from the same samples in this study.

Standard wire-line logs comprise natural gamma-ray (GR), caliper (CAL), bulk density (DEN), neutron porosity (CNL), sonic interval transit time (AC), and shallow/deep resistivity (Rxo and RT). Schlumberger's combinable magnetic resonance tool was run to acquire the nuclear magnetic resonance (NMR) T_2 spectra distribution. Therefore, information on pore structure and oil-bearing can be obtained.

Schlumberger's fullbore formation microimager (FMI) was used to obtain a high-resolution (up to 5 mm vertical resolution) pseudopicture of boreholes (Lai et al., 2020, 2021). Eight pads, four hosting pads fixed to two orthogonal arms, and each pad had an attached flap (Rajabi et al., 2010; Lagraba et al., 2010), each containing 24 buttons, was fixed on the FMI. Therefore, there were 192 electrodes distributed on four pads and four flaps, collectively generating 192 microresistivity curves (Rajabi et al., 2010; Moreau and Joubert, 2016). The colorful images were obtained through basic preprocessing workflows, including speed correction, centering correction, and normalization of the raw data (Folkestad et al., 2012; Lai et al., 2020). The borehole images were displayed as static and dynamic images that imply the electrical contrasts (Serra, 1989; Moreau and Joubert, 2016).

Usually, four white strips of missing information are invisible on the image (Bize et al., 2015). Hurley and Zhang (2011) integrated the two methods to fill these gaps to form the full images. Then, the slabs can be reconstructed using the geometrical relationships between the borehole cylinder's surface and the section's plane (Fig. 3) (Kumar et al., 2014; Bize et al., 2015). The slabs show more

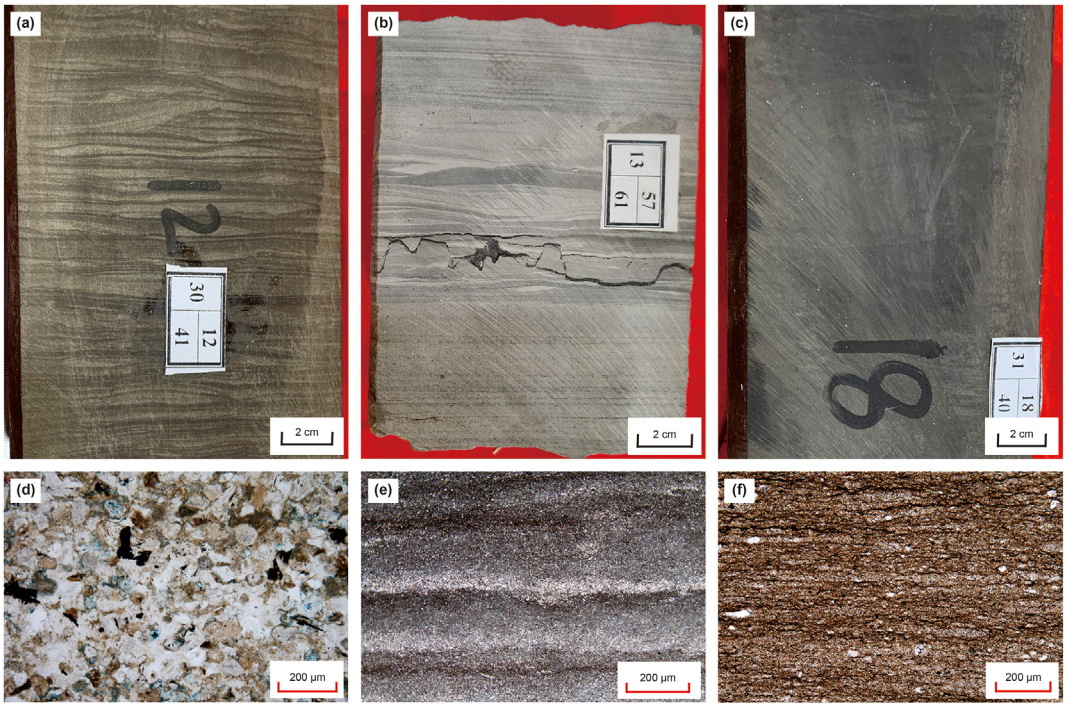

Fig. 4. Core photos and thin sections show the lithology and mineral composition in the Permian Lucaogou Formation of Jimusar Sag, Junggar Basin
(a) Siltstones, J10025, 3701.7 m
(b) Dolostones, J10025, 3539.15 m
(c) Mudstones, J10025, 3702.5 m
(d) Siltstone, quartz, feldspar and fragment, J10022, 3484.92 m
(e) Dolostone accompanied with laminae, J10022, 3489.33 m
(f) Mudstones with laminae, J10016, 3311.26 m.

geological characteristics (bedding) than the image logs (Fig. 3). The light-shaded areas of the images indicate resistive, dense, and cemented rocks, organic matter, or hydrocarbon occurrence, whereas the dark-shaded areas represent conductive clays and shale-like rocks (Khoshbakht et al., 2012; Muniz and Bosence, 2015; Lai et al., 2018a). The transitional color-shaded areas imply moderately resistive rocks, for instance, feldspar and quartz. The dominant minerals are felsic (feldspar and quartz), carbonate, clay minerals, and organic matter in the Permian Lucaogou Formation in the Jimusar Sag. Therefore, the image's color can illustrate the mineral types.

4. Results

4.1. Lithology

The lithologies of the Lucaogou Formation have been identified and classified based on mineral compositions (Xi et al., 2015; Zhang et al., 2018; Lin et al., 2021). The primary lithologies include siltstones, dolostones, and mudstones (Fig. 4a–c). Also, transitional lithologies occur, such as dolomitic siltstones, dolomicrite, and dolomitic mudstones. Interbedded siltstone and dolostones are typically in vertical contact with mudstones in the Lucaogou Formation of the Jimusar Sag (Lin et al., 2021). The complex lithologies are attributed to lake-level fluctuations, provenance, and depositional environments (Zhang et al., 2019).

The siltstones comprise feldspar, quartz, and rock fragments (Fig. 4d). Dolostones are mostly dolarenite, and the intraclast dolomites are detected by thin section analysis (Fig. 4e). Mudstones mostly consist of clay minerals and, in some cases, organic matter (Fig. 4f). Silt-sized particles of quartz and feldspar and rock fragments are identified in the siltstones (Fig. 5a).

Cores and thin section observations show that feldspar, quartz, carbonate, and clay minerals are the dominant mineral components in the Permian Lucaogou Formation (Zhang et al., 2019). Clay minerals are dominated by smectite, with moderate amounts of mixed layer illite/smectite and minor illite and chlorite.

4.2. Reservoir pore spaces

The reservoir is characterized by strong heterogeneity (Guan et al., 2020) with low porosity and permeability. According to the core-measured porosity and permeability data, the porosity is 1.2%–23.8%, and the average value is 12.5%, and the permeability is 0.01 mD to 32.9 mD and averaged as 0.9 mD. The cores and thin sections indicate that the pore spaces of the Permian Lucaogou Formation are complicated and can be divided into primary intergranular pores (Fig. 5a), secondary dissolution pores (Fig. 5a–c), and fractures/microfractures (Fig. 5d–f).

Primary intergranular pores include the residually primary intergranular pores preserved after mechanical compaction, enlarged by dissolution, forming mixed pores that primarily exist in the siltstones (Fig. 5a). These pores are the main contributors to the porosity of the Lucaogou Formation in the Jimusar Sag. However, some are filled with authigenic quartz, carbonate cement, and other minerals (authigenic clay minerals), reducing the reservoir's quality (Fig. 5g and h). Secondary pores are crucial reservoir spaces in the Lucaogou Formation and are observed in most lithologies, especially sandstones and dolostones. Secondary pores are primarily intragranular dissolved pores within framework grains, such as feldspar and rock fragments. Microfractures developed with sparry carbonate crystals and organic matter precipitated in the microfracture planes (Fig. 5e and f).

Natural fractures are vital reservoir spaces and seepage channels in hydrocarbon reservoirs, and they play a significant role in controlling the exploration and development potential of tight/shale oil play (Lai et al., 2022a). Fractures can be divided into bedding parallel and inclined (tectonic) fractures. Studies have shown that bedding fractures developed along the bedding planes (Zhang et al., 2017; Liu et al., 2019a). The fractures in the Lucaogou Formation are further divided into open and closed fractures based on whether they are cemented. The formation of fractures could be the tectonic origin, hydrocarbon generation, accumulation, and diagenesis (Zeng and Li, 2009; Lai et al., 2016; Zhang et al., 2017; Liu et al., 2020). The fractures not cemented by cements such as calcites, i.e., open fractures, will be hydrocarbon storage spaces (Gale et al., 2007, 2014; Kuang et al., 2012; Ghanizadeh et al., 2015;

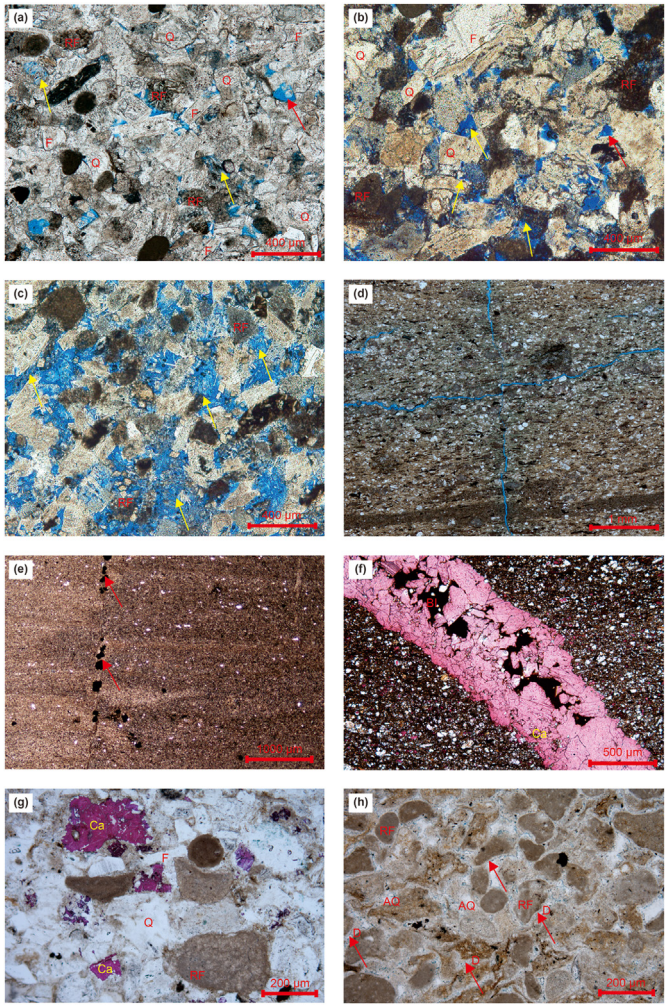

Fig. 5. Thin section images showing the lithology and pore spaces of the Lucaogou Formation in the Jimusar Sag
(a) Siltstones with primary intergranular pores (red arrows) and intragranular dissolution pores (yellow arrows), J10025, 3554.83 m
(b) Intergranular dissolution pores and intragranular dissolution pores due to various degree of grain dissolution, J10016, 3314.12 m
(c) Abundance of intergranular pores and intragranular dissolution pores, low to moderate degree of compaction, J10025, 3541.79 m
(d) Microfractures paralleled and vertical to lamina, J10025, 3571.73 m
(e) Extensive compaction and microfractures with filling of pyrite and bitumen, J10016 3311.88 m
(f) Parallel fractures filled of cementation of calcite and dolomite, J10022, 3475.54 m
(g) Fine-grained sandstones with metasomatism of calcite, J10016, 3312.35 m
(h) Dolomite with authigenic quartz, J10016, 3325.22 m
Q, quartz; RF, rock fragments; F, feldspar; Ca, Calcite; D, dolomite; AQ, authigenic quartz. BI, bitumen.

Hooker et al., 2015; English and Laubach. 2017; Liu et al., 2020), and they will become migration channels for fluids. Dissolved ions carried by fluids will precipitate as diagenetic minerals during fluid migration due to temperature and pressure changes (Zhang et al., 2017).

Moreover, SiO_2 migration results in quartz precipitation, whereas $CaCO_3$ migration results in calcite precipitation and cementation (Cao et al., 2016; Kuang et al., 2012; Ghanizadeh et al., 2015). Some microfractures were filled with asphalt, calcite, pyrite, and other minerals (Fig. 5e and h). Many tectonic fractures and microfractures in the Permian Lucaogou Formation were filled with cement, such as calcite, clay, or quartz. Precipitation and cementation will reduce the fracture effectiveness and decrease the value of porosity and permeability (Bennett et al., 1991). In the thin section observation, microfractures were mostly near-parallel to the lamina surfaces (Fig. 5d and f).

The fractures parallel to the bedding planes in the reservoirs were often oil-bearing, indicating hydrocarbon accumulation (Zhang et al., 2017). Cross, horizontal, and oblique beddings are structurally weak surfaces that facilitate fracture formation (Liu et al., 2020).

Feldspar dissolution (Fig. 5c) and carbonate cementation (Figs. 4d, 5e and 5g) were the two dominant diagenetic modifications, causing heterogenization of the fine-grained sedimentary rock reservoir (Lin et al., 2021). Feldspar dissolution occurred in pyroclastic laminae with low carbonate contents and was caused

Fig. 6. Core photos showing the lithology and the three types of lamina structure of the Lucaogou Formation in the Jimusar Sag
(a) Massive mudstone, J10012, 3157.30 m
(b) Massive dolostone, J10025, 3607.50 m
(c) Layered dolostone, J10025, 3699.58 m
(d) Layered sandstone, J10022, 3313.36 m
(e) Layered dolostone, J10025, 3687.74 m
(f) Laminated siltstone, J10025, 3714.85 m
(g) Laminated dolostone, J10025, 3696.54 m
(h) Laminated dolostone, J10025, 3675.38 m.

by organic acid-rich fluids. Carbonate cementation occurs in carbonate laminae (Lin et al., 2021). The carbonate particle dissolution by organic acids and CO_2 provides the material sources for secondary carbonate cements (Lin et al., 2021). The Ca^{2+} and Mg^{2+} ions produced by transforming smectite to illite in the laminae also provide material sources for secondary carbonate cements (Lin et al., 2021).

4.3. Multiscale laminae structure

The core and thin section observations show that laminated rocks with rhythmic bedding are common in the Lucaogou Formation. Rocks with different felsic mineral contents are frequently alternated vertically. Even in rocks with similar felsic mineral contents, the carbonate, clay, and organic matter contents are varied considerably (Lin et al., 2021).

4.3.1. Division of multiscale laminae patterns

Lamina refers to the smallest or thinnest original sedimentary layer that can be distinguished in sediments or sedimentary rocks (Li et al., 2018). The slabs derived from the image logs are employed to describe the laminae characteristics. A single layer's thickness is typically less than 10 mm, and the lamina of shale is 0.02 mm–1 mm (Li et al., 2018; Zhu, 2021). The definition of lamina is extended, and the minimum level of lamina that can be identified from relevant observation means at a certain scale is defined as the lamina at that scale (Li et al. 2017, 2018). Therefore, multiscale laminae from meter to millimeter can be identified from macro–meso–microscopic observations (Li et al. 2017, 2018). In our study, we divided the lamina structure into laminated rocks (millimeter-scale; single layer thickness is less than 1 cm), layered rocks (centimeter-scale; single layer thickness is 1–10 cm), and massive rocks (decimeter-scale; single layer thickness is larger than 10 cm). Conventional logs can identify the meter–decimeter-scale lamina, and the image logs, especially the slabs derived from the image logs, can identify the millimeter–decimeter-scale lamina. Core observations can identify the centimeter–millimeter-scale lamina, and the thin section can identify the millimeter–micrometer-scale lamina.

Regarding the scale of laminae patterns, the lamina structure on the core can be divided into 1) massive (no layer or the layer spacing is > 0.1 m) (Fig. 6a and b), 2) layered (the thickness of an

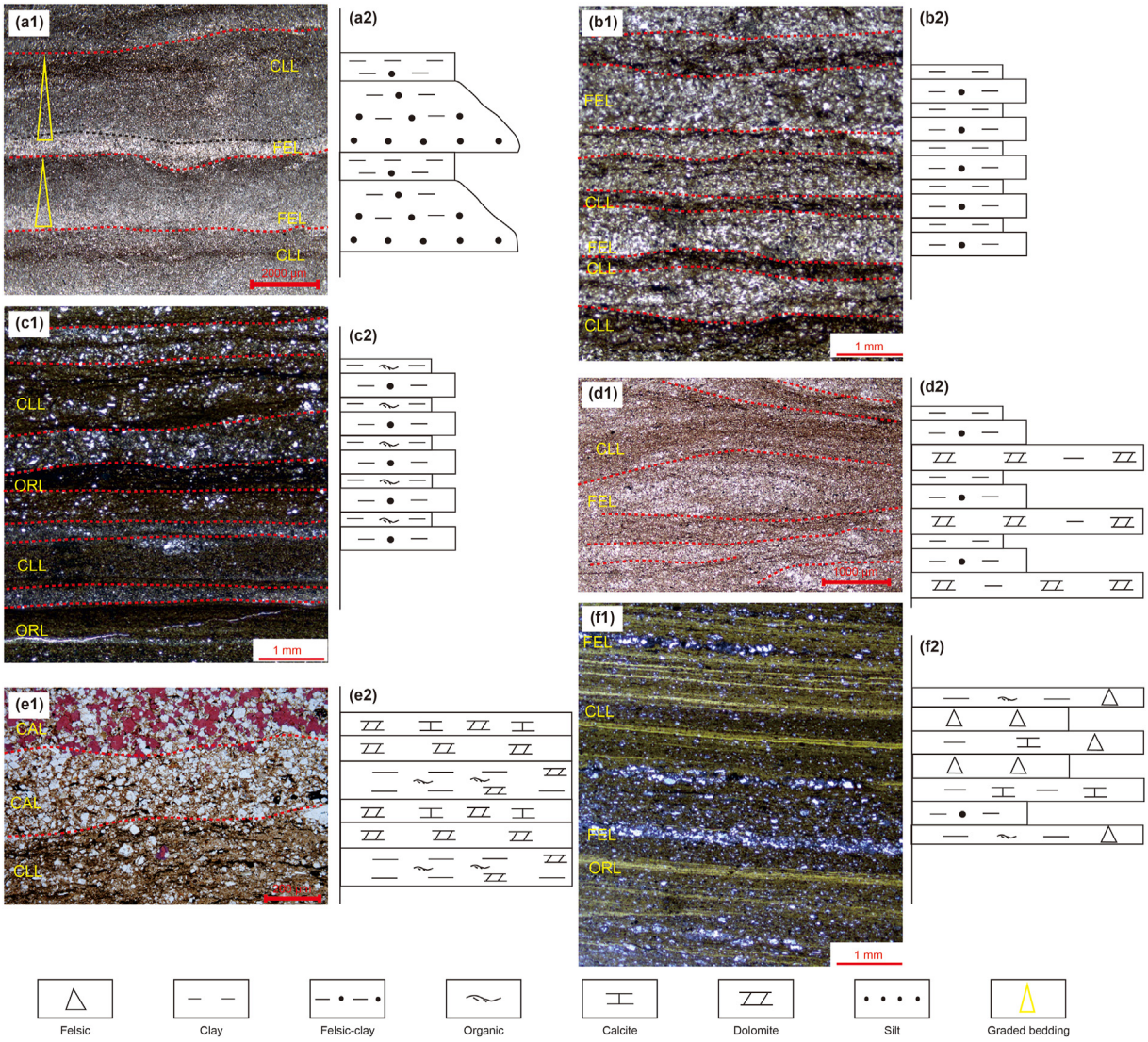

Fig. 7. Four types of lamina composition patterns in the Permian Lucaogou Formation in the Jimusar Sag
Abbreviation: FEL felsic lamina; CAL carbonate lamina; CLL clay lamina; ORL organic lamina.

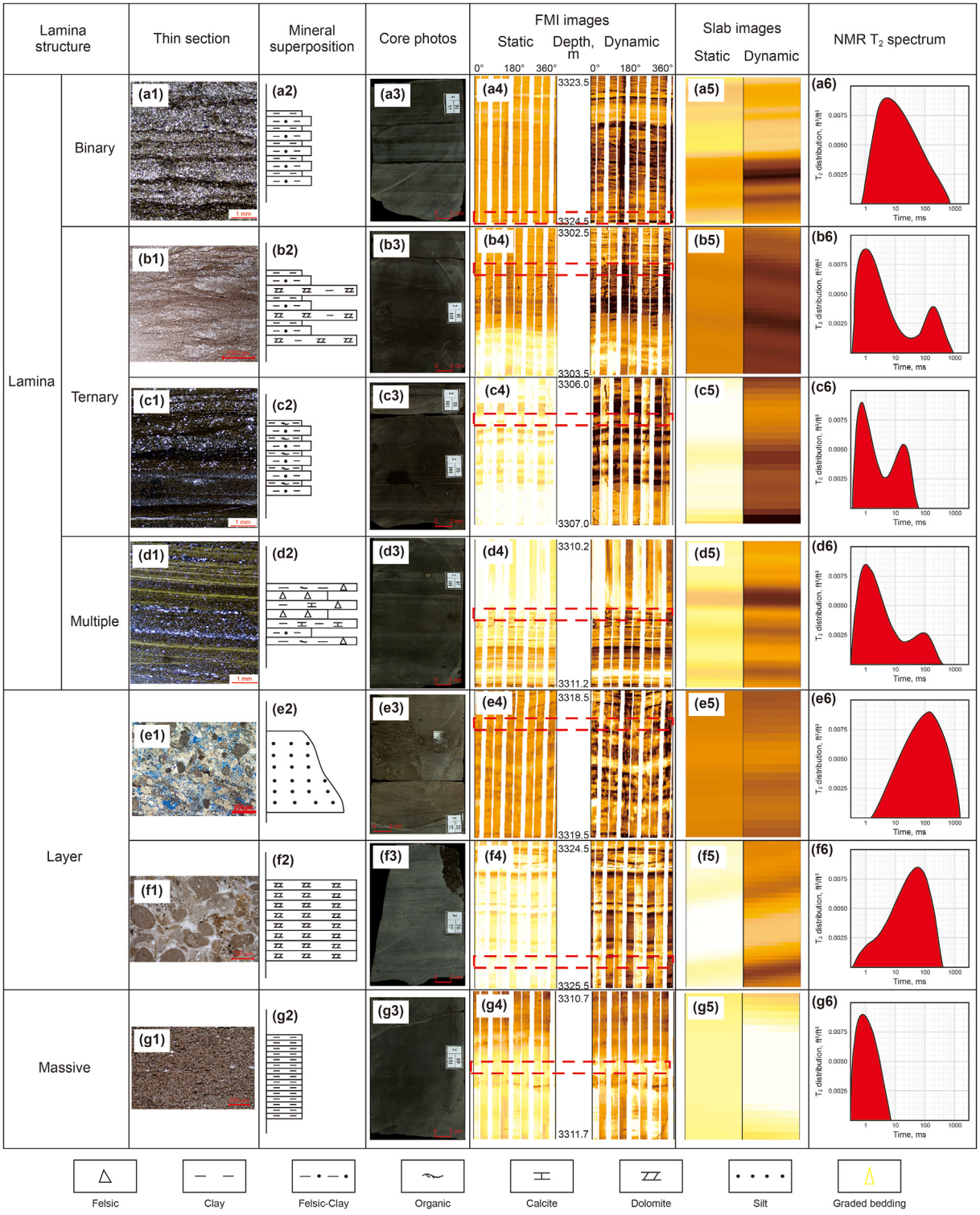

Fig. 8. Lamina structure types interpreted from core photos and thin sections as well as relative well log response characteristics (NMR, slabs and image) of the Lucaogou Formation in the Jimusar Sag

(a1), thin section, J10016, 3324.3 m, binary lamina (felsic, clay) with the homologous diagram (a2), core photo (a3), and the corresponding of image log (a4) and slab (a5), the NMR T_2 spectrum of this kind of lamina (a6).

(b1), thin section, J10016, 3302.8 m, ternary lamina (felsic, clay, carbonate) with the homologous diagram (b2), core photo (b3), and the corresponding of image log (b4) and slab (b5), the NMR T_2 spectrum of this kind of lamina (b6).

(c1), thin section, J10016, 3306.3 m, ternary lamina (felsic, clay, organic) with the homologous diagram (c2), core photo (c3), and the corresponding of image log (c4) and slab (c5), the NMR T_2 spectrum of this kind of lamina (c6).

(d1), thin section, J10016, 3310.8 m, multiple lamina (felsic, clay, carbonate, organic) with the homologous diagram (d2), core photo (d3), and the corresponding of image log (d4) and slab (d5), the NMR T_2 spectrum of this kind of lamina (d6).

(e1), thin section, J10016, 3318.69 m, layered rocks of stratified argillaceous sandstone with the homologous diagram (e2), core photo (e3), and the corresponding of image log (e4) and slab (e5), the NMR T_2 spectrum of this kind of lamina (e6).

(f1), thin section, J10016, 3325.22 m, layered rocks of stratified dolomite with the homologous diagram (f2), core photo (f3), and the corresponding of image log (f4) and slab (f5), the NMR T_2 spectrum of this kind of lamina (f6).

(g1), thin section, J10016, 3311.3 m, massive rocks with the homologous diagram (g2), core photo (g3), and the corresponding of image log (g4) and slab (g5), the NMR T_2 spectrum of this kind of lamina (g6).

individual layer is 0.01–0.1 m) (Fig. 6c–e), and 3) laminated (the thickness of an individual layer is < 0.01 m) (Fig. 6f–h), which have various responses on image logs (Wang et al., 2021). Overall, the more developed the laminae, the better the physical properties of the reservoir.

The massive rocks have no evident beddings or layers, and the lithologies comprise mudstones or dolomitic mudstones (Fig. 6a and b), deposited in a low hydrodynamic environment, indicating unique mineral components. Lamina cannot be seen in thin sections in this type of rock, and the layered rocks are associated with siltstones and dolostones (Fig. 6c–e). Evident beddings or layers have developed, and the scales are 0.01–0.1 m (layer spacings). Thin sections can confirm the layered rocks (Fig. 7), and the laminated rocks can be siltstones, dolostones, and, in some cases, mudstones (shales) (Fig. 6f–h). The thin section observations reveal the laminated rocks in the siltstones (Fig. 6f), dolomitic mudstones (Fig. 6g), and dolostones (Fig. 6h). The laminated rocks were deposited in a dynamic environment with seasonal climate and sediment supply changes, resulting in rapid changes in mineral components and forming laminated structures (Liu et al., 2019a; Xi et al., 2020).

4.3.2. Mineral composition of laminae

Besides core observation, thin sections can be used for millimeter–micrometer-scale lamina structure determination and for recognizing the mineral superimposition patterns. The thin section can be employed to determine the mineral superimposition sequences for the laminated rocks. Four laminae types (individual mineral compositions) are identified in the laminated rocks in the Lucaogou Formation in the Jimusar Sag: 1) felsic lamina (quartz, feldspar), 2) carbonate lamina, 3) organic matter lamina, and 4) clay mineral lamina.

The felsic laminae contain feldspar, quartz, and minor rock fragments (Fig. 7a and b). Clay minerals (Fig. 7a–f) and carbonate minerals (Fig. 7e) (calcite and dolomite) appeared as matrix and cement filling between the particles, respectively. The organic matter is distributed between the particles in spotty or dispersed form. Graded bedding can be seen in the felsic laminae when the felsic content changes within a specific range (Fig. 7c and f).

Under the same thermal evolution condition, samples with high organic matter abundance have evident hydrocarbon generation and pressurization effects, and the abnormal pressure fractures are moderately developed (Zhang et al., 2017; Liu et al., 2020). As brittle

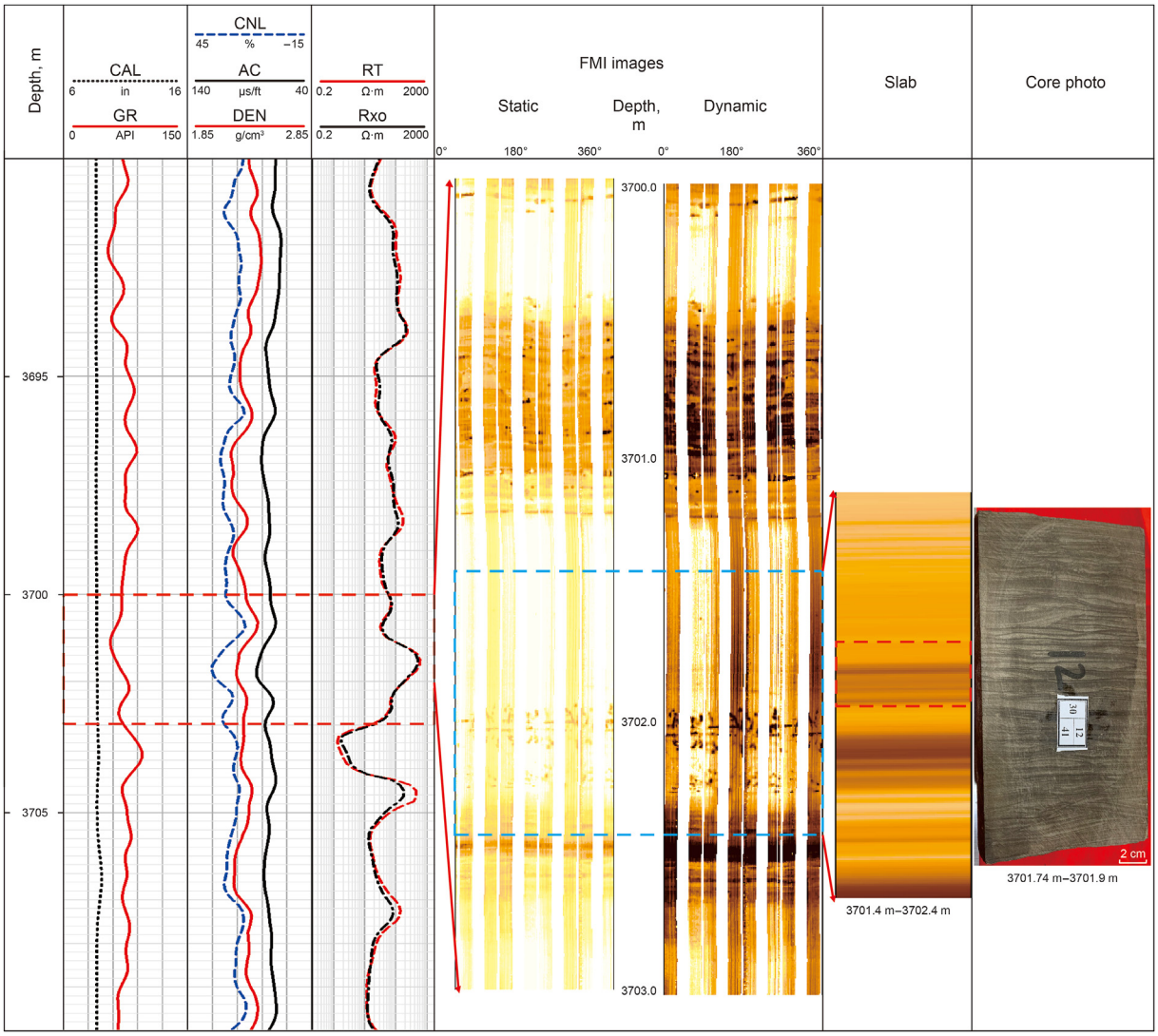

Fig. 9. Well log expression and related core photo of laminated rocks
The first track shows the depth, and the second are the natural gamma rays (GR) and caliper (CAL). The third track include the three porosity logs (AC, CNL and DEN), respectively and the fourth track shows deep resistivity (RT) and shallow resistivity (Rxo) log. The fifth track is FMI images with the related slab in the sixth track. The seventh track is core photo.

minerals, the higher the quartz and feldspar contents, the higher the rock's brittleness. However, when the felsic is dispersedly distributed in the rock, it will cause stress dispersion during hydraulic fracturing, which is inconducive to network fracture formation (Liu et al., 2018).

The carbonate laminae comprise calcite and dolomite, and the organic matter is in the morphology of the strip and distributed dispersedly with clay minerals (Fig. 7e). The laminae interfaces are relatively straight and continuous (Fig. 7e). When the clay mineral content is moderately high, the carbonate laminae interface is wavy (Fig. 7e), indicating that the sedimentary hydrodynamics are strong during the sedimentary period (Xi et al., 2020). However, the cementation of carbonate minerals might reduce the reservoir spaces.

The organic matter laminae consist of the organic-rich lamina (Fig. 7f) and are recognized as black layers under microscopic observation. The deposition thickness of a single organic lamina is very thin and exists in the form of strips in other layers or coexists with other components, such as felsic layers. Furthermore, the organic matter laminae interface is wavy or intermittent (Fig. 7c and f).

The clay laminae are mainly composed of clay minerals, which are brown to gray-black under the microscope (Fig. 7c and d). The clay laminae interface is straight and continuous and often forms a binary laminated combination with felsic layers. Because clay minerals are easy to be compacted during the burial history, the reservoir quality will be poor due to the late stage of burial diagenetic modifications.

4.3.3. Mineral superimposition patterns

The lamina structure can be divided into three scales: massive, layer, and lamina regarding core observations (Fig. 6). Furthermore, the laminated rocks can be further divided into three subtypes according to the mineral superposition assemblages: 1) binary (superposition of two minerals), 2) ternary (superposition of three minerals), and 3) multiple (superposition of more than three minerals). Thin section observations and related NMR tests show that the lamina rocks have varied pore spaces and NMR T_2 distributions (Fig. 8). The layered rocks have better oil content and physical properties than the laminated and massive rocks (Fig. 8).

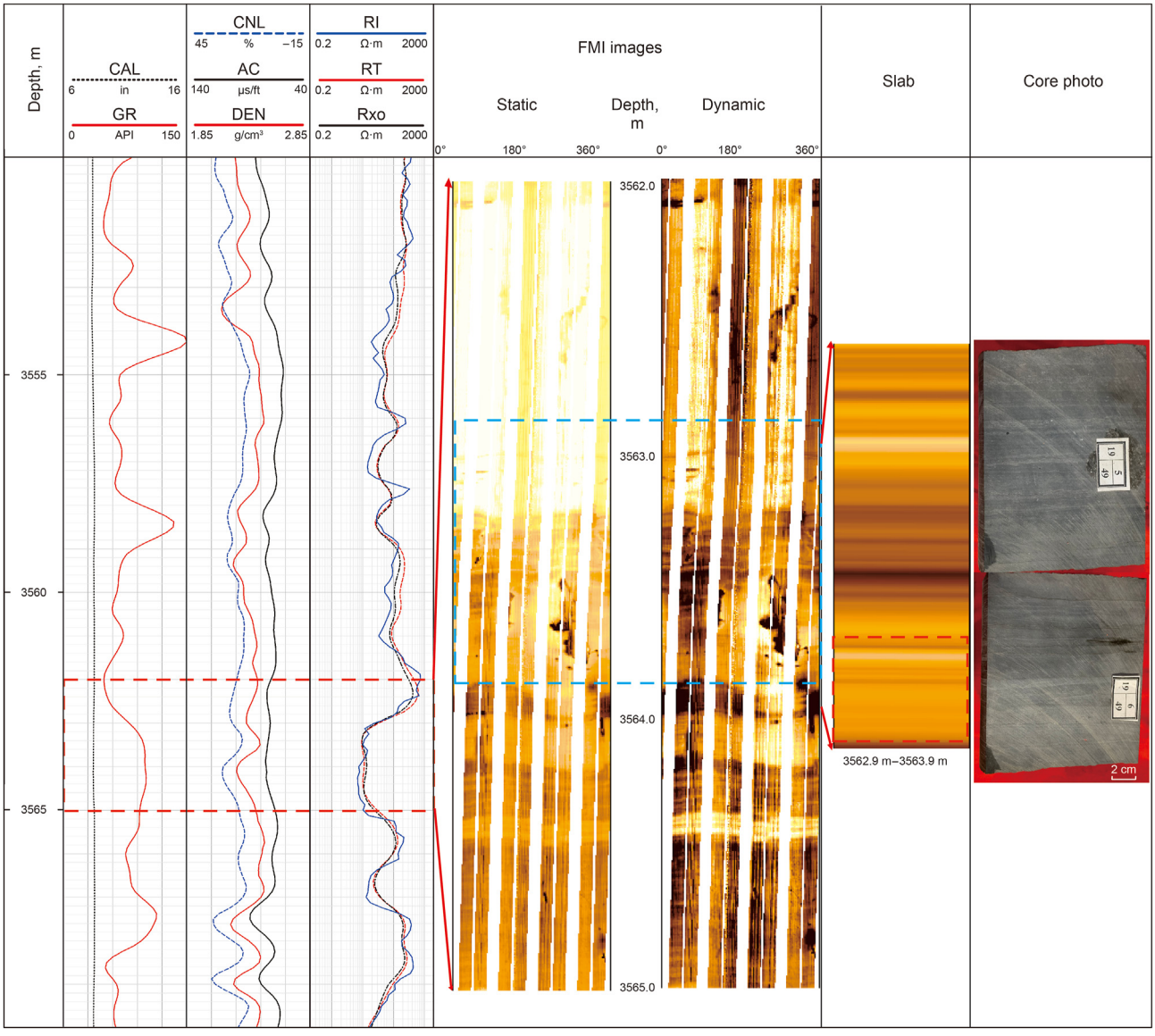

Fig. 10. Well log expression and related core photo of layered rocks.

Furthermore, the binary, ternary, and multiple lamina types varied in reservoir quality (Fig. 8).

The binary lamina (felsic, clay) has wave laminae with a clear boundary (Fig. 8a1–a2). When the felsic mineral content is high, normal graded bedding inside the felsic lamina indicate that the sedimentary energy gradually weakened during the deposition period. The lamina interfaces between the two lamina types are well-clear and near-flat or corrugated (Fig. 8a1). The organic matter content in the felsic laminae is low. The core of binary lamina (felsic, clay) shows a deep gray-brown (Fig. 8a3). The high NMR T_2 signal amplitudes and long T_2 components indicate high reservoir quality and oil-bearing potential (Golsanami et al., 2014). Dark (clay mineral) and yellow-orange (felsic mineral) layers can be observed on the image logs (Fig. 8a4), and the slabs are characterized by two-color patterns (Fig. 8a5). This type of laminae has medium physical properties and favorable oil content (Fig. 8a6) and is common in the Lucaogou Formation in the Jimusar Sag.

The ternary lamina structure comprises three superposed minerals. The first type is the superposition of felsic, carbonate, and clay minerals. The related core of the ternary lamina (felsic, carbonate, clay) is dark brown (Fig. 8b1–8b3). Gray-white felsic minerals might appear in lenticular, and the thin layers of moderately dark gray-brown-gray clay, gray felsic minerals, and white carbonate laminae are interbedded (Fig. 8b1). The boundary between various laminae is unclear, and the interfaces between the two types were not flat (Fig. 8b1). The image log shows a layered mode (Fig. 8b4), and the slab shows a bright carbonate interbedded with orange felsic and black clay laminae (Fig. 8b5). The ternary lamina (felsic, carbonate, clay) has high physical properties and oil-bearing potential (Fig. 8b6).

Another type of ternary lamina structure is the superposition of felsic, clay, and organic laminae (Fig. 8c1, 8c2) with a dark brown core (Fig. 8c3). The organic matter and clay mineral lamination are dispersed in intermittent form and are near-parallel (Fig. 8c1), and the lamination interfaces between the two types are clear (Fig. 8c1). The image logs are characterized by dark-yellow and bright layers (Fig. 8c4), and three color patterns occur in the slabs (Fig. 8c5). This type of laminae has poor physical properties with lower felsic

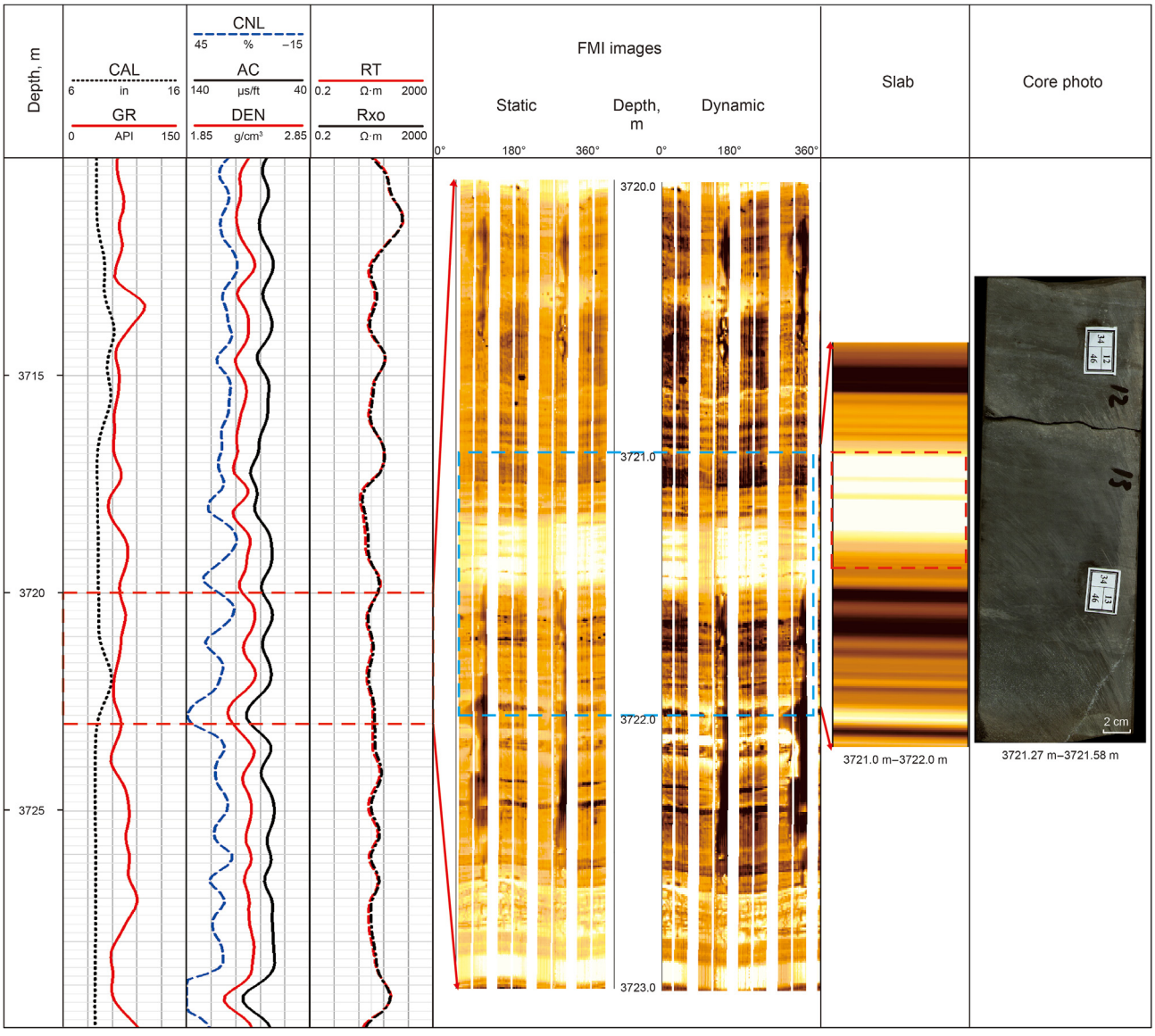

Fig. 11. Well log expression and related core photo of massive rocks.

mineral content, as determined from the NMR T_2 spectrum (Fig. 8c6). The organic matter was distributed in dispersed form in carbonate laminae (Fig. 7e). However, the organic matter was distributed near-continuous or intermittent in the clay laminae (Fig. 7e), and this type is also common in the Lucaogou Formation.

The felsic mineral content was moderately high in the multiple laminae (felsic, clay, carbonate, and organic matter), followed by carbonate and clay minerals (Fig. 8d1–8d3). The layer is moderately straight, the interfaces between the two types of laminae are unclear, and the vertical change is different in color (Fig. 8d1). The carbonate lamination was intermittent or continuous in a flat form parallel to other laminae (Fig. 8d1). The image logs and related slabs show typical color pattern changes due to the rapid mineral component changes (Fig. 8d4, 8d5). This lamina structure was poor with low oil saturation (Fig. 8d6) and was rare in the Lucaogou Formation.

Layered rocks are associated with siltstones (Fig. 8e1–8e3) and dolostones (Fig. 8f1–8f3), with quartz and feldspar being the main mineral components. Intergranular and intragranular pores can be identified in the casting dyeing thin sections (Fig. 8e1), and the layered dolostones might contain no evident pore spaces (Fig. 8f1). The layered structure can be observed on the image logs and slabs (Fig. 8e4, 8e5; Fig. 8f4, 8f5). The layered siltstones have high physical properties, as determined by high NMR T_2 signal amplitudes and long T_2 components (Fig. 8e6). The framework grains are well-sorted and moderately texturally mature, subrounded to rounded shapes, and have line-to-face contacts in the stratified dolomite (Fig. 8e1, 8f1). The physical and oil-bearing properties of the layered dolostones were satisfactory (Fig. 8f6). Conversely, evident layers or laminae can be detected on the image logs for the layered rocks (Fig. 8).

Massive rocks comprise mudstone, dolostone, and in some cases, dolomitic siltstone (Lin et al., 2021). The massive mudstone is rich in organic matter (Fig. 8g1–8g3), with the characteristics of a

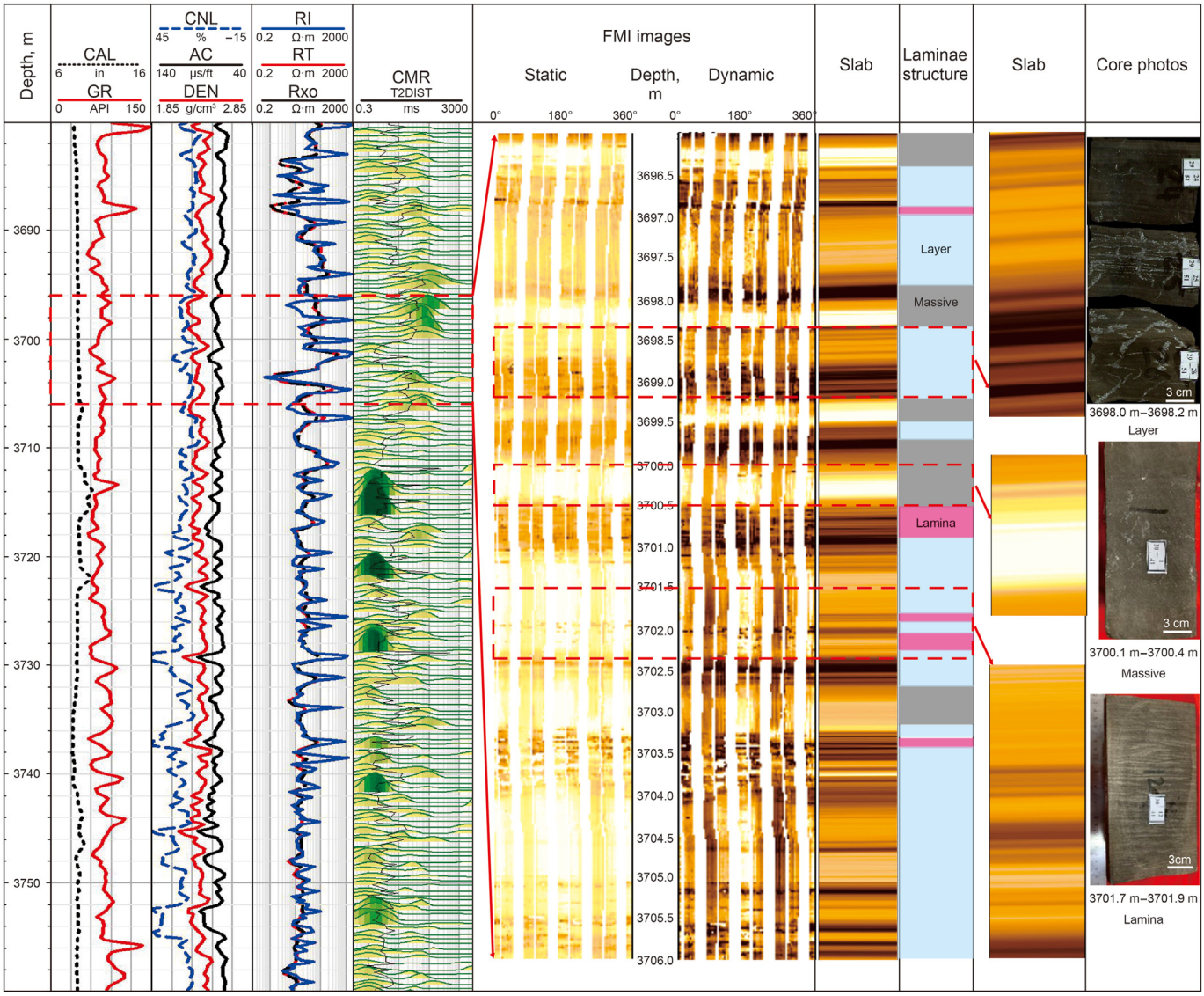

Fig. 12. Identification and classification of multi-scale laminae structure of the Lucaogou Formation in J10025
The first track shows the depth, and the second are the natural gamma rays (GR) and caliper (CAL). The third track include deep resistivity (RT) and shallow resistivity (Rxo) log and the fourth track shows the three porosity logs (AC, CNL and DEN), respectively. The fifth track shows the T_2 spectrum of CMR, and the sixth track is FMI images with the relevant slab in the seventh track and the eighth track shows three types of lamina structure. The ninth track exhibits the representative lamina structure with the related core photos in the tenth track.

dark color, interpreted to deposit under the deep to the semi-deep lacustrine environment (Yang et al., 2019; Zhang et al., 2019). Abundant micritic dolomites were observed in the dolostone. Furthermore, massive rocks are formed by carbonate with micritic dolomites and dolomitic intraclast components (Fig. 8g1). No layers or bands can be observed on the image logs for the massive type, and the slabs show no color pattern variations (Fig. 8g4–8g5). The reservoir quality and oil-bearing properties are poor, as observed from the low T_2 amplitudes and dominance of short T_2 components (Fig. 8g6).

Laminated rocks (binary, ternary, and multiple mineral superposition assemblages) have the highest layer and lamina density on the FMI image and slabs (Fig. 8a5, 8b5, 8c5, 8d5), followed by layered rocks (Fig. 8e5, 8f5). The massive rocks appear bright or dark on the image logs and slabs (Fig. 8g5). Reservoirs with developed laminae rocks have medium physical properties (Fig. 8a6, 8b6, 8c6, 8d6). The layered rocks are characterized by the highest T_2 amplitudes and the longest T_2 components in the NMR T_2 spectra (Fig. 8e6, 8f6), indicating favorable physical properties and high movable fluid contents. The massive rocks have the lowest T_2 amplitudes, and the T_2 spectrum is characterized by unimodal and left-skewed, indicating poor reservoir quality and oil-bearing properties (Fig. 8g6).

The more the laminae of brittle siliceous minerals are, the better the fracture ability of the reservoir (Lei et al., 2015). The continuity, shape, and geometry of the laminae boundary directly influence the propagation law of fractures during reservoir fracturing (Sun et al., 2020; Shi and Qiu, 2021). The lamina composite structure with continuous, straight, and clear boundaries can easily form a network fracture during fracturing. However, the laminae are discontinuous, not straight, and the boundary is unclear. The pressure will be dispersed during fracturing, and complex network fractures will be formed. Simultaneously, the laminae boundary's angle will affect the rock's mechanical properties. The uniaxial compressive strength increases with the lamina angle, and the correlation between them is linear (Xu et al., 2015; Xiong et al., 2019; Shi and Qiu, 2021). Bedding plane cracking and fracture path deviation are the main causes of anisotropy of the fracture toughness (Xu et al., 2015; Xiong et al., 2019; Heng et al., 2020; Shi and Qiu, 2021).

4.4. Well log responses

Conventional well logs could identify the meter–centimeter-

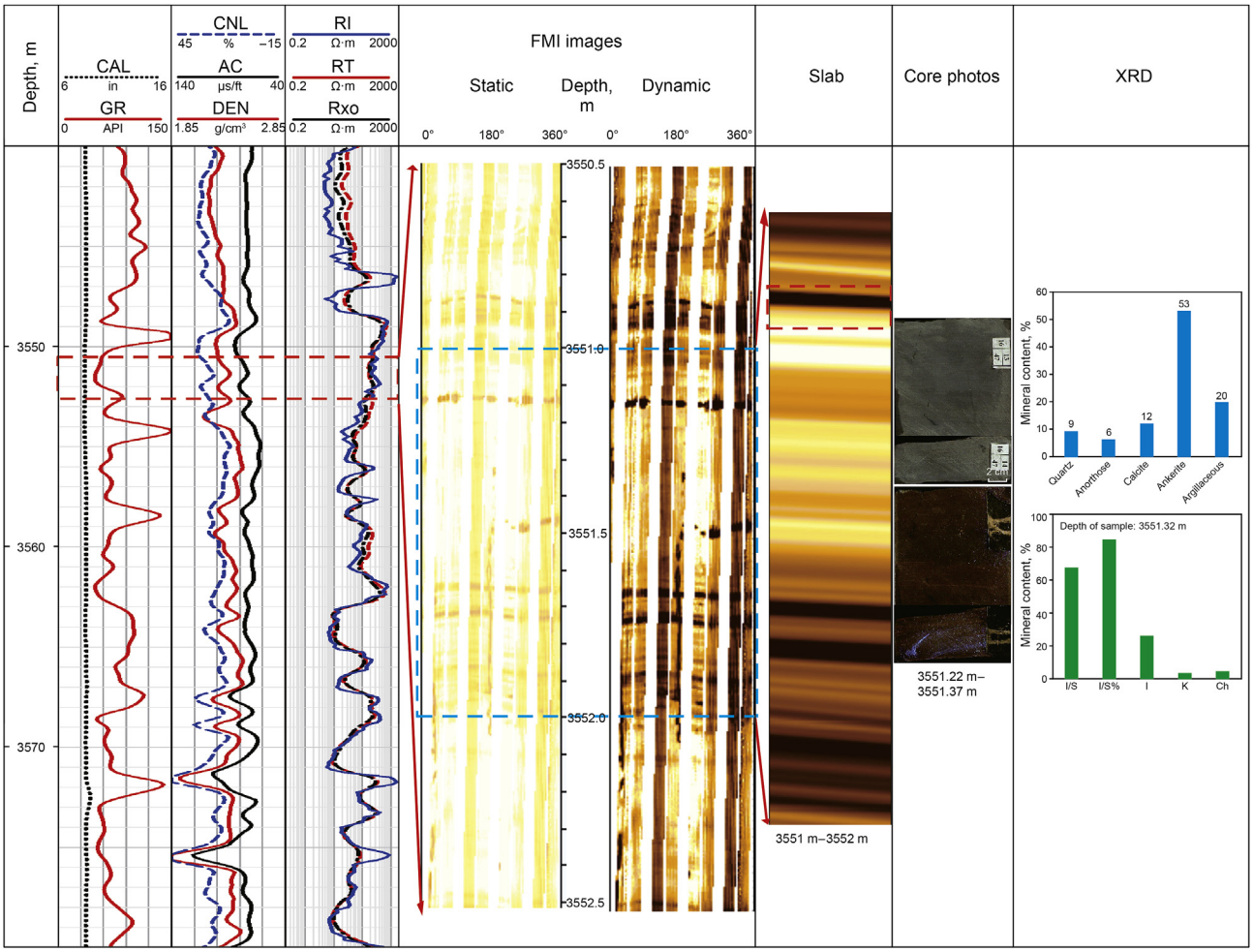

Fig. 13. Well log expression of binary lamina (carbonate, clay) in the Lucaogou Formation in the Jimusar Sag
The first track shows the depth, and the second are the natural gamma rays (GR) and caliper (CAL). The third track include the three porosity logs (AC, CNL and DEN), respectively and the fourth track shows deep resistivity (RT) and shallow resistivity (Rxo) log. The fifth track is FMI images with the related slab in the sixth track. The seventh track is core photos. And the eighth track is XRD.

scale of lamina assemblages, which cannot meet the resolution standard of exploration in tight/shale oil reservoirs. Due to the high costs, the cores and thin sections cannot be available in each well and depth. Consequently, the high-resolution characteristics of the image log (5 mm or 0.2 in) can help divide the layered, laminated, and massive rocks ranging from millimeter to meter scales.

The dynamic slabs of the image logs show that the laminae are alternately light and dark, and the laminated rocks show that a single layer's thickness is in millimeter scale, less than 1 cm, indicating that the laminae changes are millimeter lamination. Fig. 9 shows more than 124 layers in different colors in 1 m (Fig. 9). An individual layer's thickness is centimeter-scale in the layered rocks (1–10 cm), and 65 layers in 1-m ranges are identified on the slabs (Fig. 10).

The single layer of massive rocks is in decimeter–meter scale and the layer thickness is greater than 10 cm, or there are no layers in the massive rocks. Typically, the image logs and the slabs are characterized by a single dark or bright spot, and no layers can be detected at 0.1 m scale depth intervals (Fig. 11).

5. Discussion

5.1. Laminae distribution prediction via well logs

The bright, orange, or dark appearances on the image logs and related slabs depend on the mineral composition variations. For instance, the massive rocks are characterized by bright or dark appearances (Fig. 11), the layered rocks are characterized by alternating dark and bright bands (Fig. 10), and the laminated rocks are recognized by laminae characteristics showing dark, orange-yellow, and bright color patterns (Fig. 9).

Therefore, the division of laminae structure in a single well can be realized through the image logs and related slabs (Fig. 12), and 528 layers have been identified in Well J10025 of the Lucaogou Formation, among which 119 intervals are laminated rocks, 259 are layered rocks, and 149 are massive rocks. The laminated rocks' thickness reached 37.92 m, with a minimum thickness of 0.06 m and a maximum thickness of 2.57 m. The layered rocks' entire thickness is 242.19 m, the minimum thickness is 0.04 m, and the maximum thickness is 8.21 m. The massive rocks' total thickness is 30.31 m, the minimum thickness is 0.1 m, and the maximum thickness is 1.32 m (Fig. 12). The effective combination of clay and felsic minerals results in a large amount of oil and gas migration into the felsic layers (Shi and Qiu, 2021).

The lamina structure subtypes (binary, ternary, and multiple) in laminated rocks can be identified through the slabs' image pattern and color gradation. The binary laminated type is dominated by carbonate and clay minerals and has a high carbonate content, moderately low clay mineral content, and few felsic layers, evidenced by the XRD data (Fig. 13). Core observations show that the

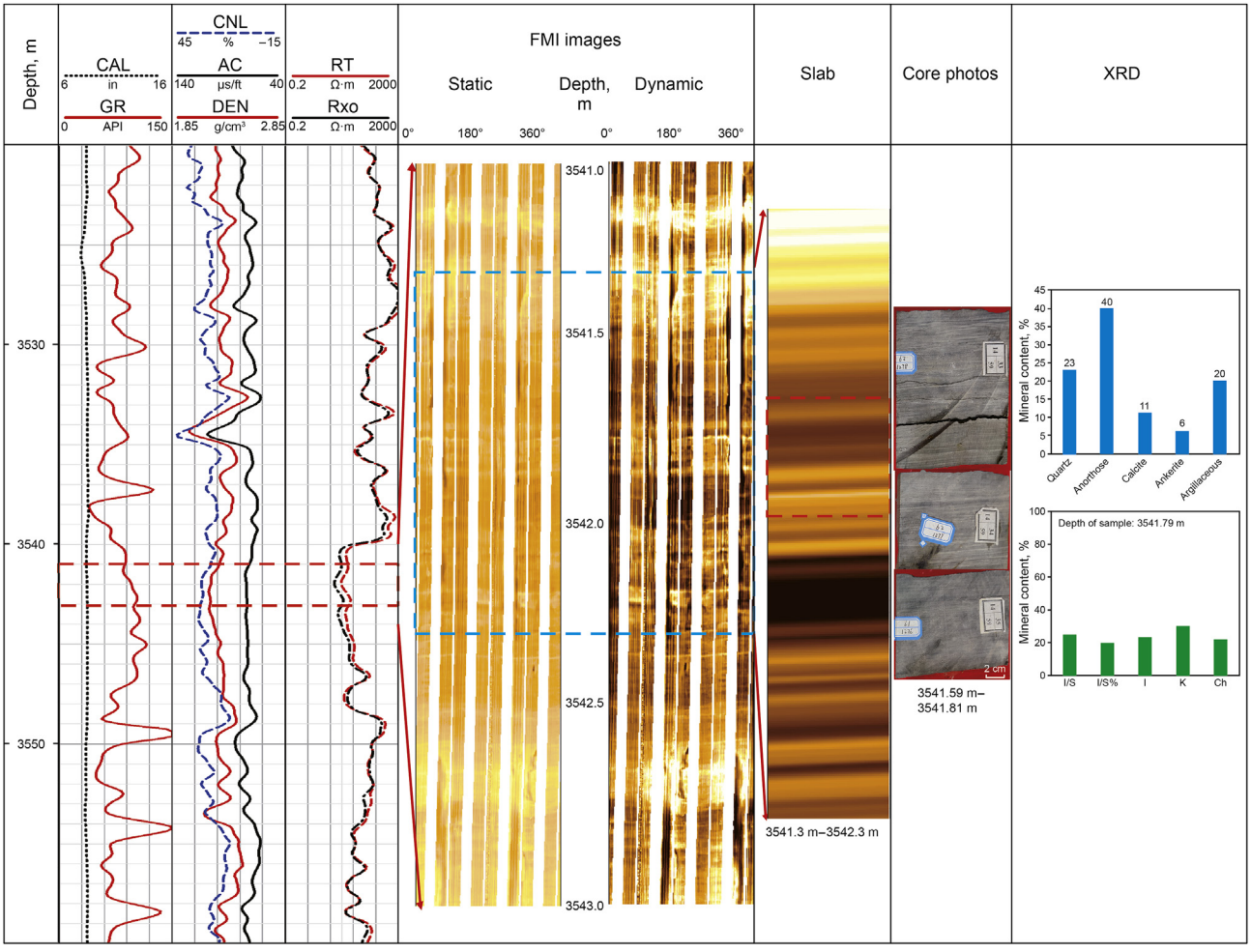

Fig. 14. Well log expression of ternary lamina (felsic, carbonate, clay) in the Lucaogou Formation in the Jimusar Sag.

color patterns of the binary laminated type are gray to brow-gray. The image logs have typical alternating band characteristics due to the mineral variations. Furthermore, the slab is recognized as a dark layer (clay mineral lamina) and a bright layer (carbonate lamina) (Fig. 13).

In laminated rocks, the ternary laminae combination (felsic, carbonate, clay mineral) has high felsic content and moderately low clay and carbonate mineral contents. The gray-white felsic minerals are lenticular, intermittently layered, or thinly layered interlayers with dark gray to brown-gray clay–carbonate laminae. The image log is band facies, and the slab is a dark layer (clay lamina), a light layer (carbonate lamina), interlayered with an orange layer (felsic lamina) (Fig. 14).

Another type of ternary lamina combination in laminated rocks comprises felsic, clay, and organic matter. It has higher felsic content, followed by clay minerals and some organic matter, but no carbonate lamina, as evidenced by the XRD data (Fig. 15). The slab of this lamina structure is characterized by interbedded color patterns of an orange-yellow layer (felsic lamina), a dark layer (clay lamina), and a light layer (organic lamina) (Fig. 15). Even though organic matter and carbonate minerals show bright characteristics on the slab, there is differentiation on the conventional well log. The organic matter has medium to high GR, whereas the GR value is low for carbonate minerals. The lamina boundary is straight, and the black organic matter is dispersed along the bedding in the thin section observation (Fig. 7b and e). Reservoirs with ternary lamina (felsic, clay, and organic matter) have high oil saturation (Fig. 15).

The felsic content is moderately high, followed by carbonates, clay minerals, and organic matter in the multiple lamina types (Fig. 16). The laminae are straight, and their boundaries are unclear (Fig. 7f). The vertical change shows different colors due to seasonal, cyclical climate changes. The appearance of tiny amounts of felsic laminae proves that the originally quiet deep lake area can be affected by strong terrestrial input under certain conditions, destroying the original clay and carbonate seasonal laminae. The physical properties are poor, and the oil saturation is low in the reservoir (Fig. 16).

Image logs and related slabs color changes can identify and divide lamina types of different scales in the vertical section (Fig. 17). The laminated, layered, and massive rocks are first divided according to the image logs, slabs, and core observation (Fig. 17). Then, the binary, ternary, and multiple laminae are divided according to the image logs, slabs, and the thin sections observation (Fig. 17).

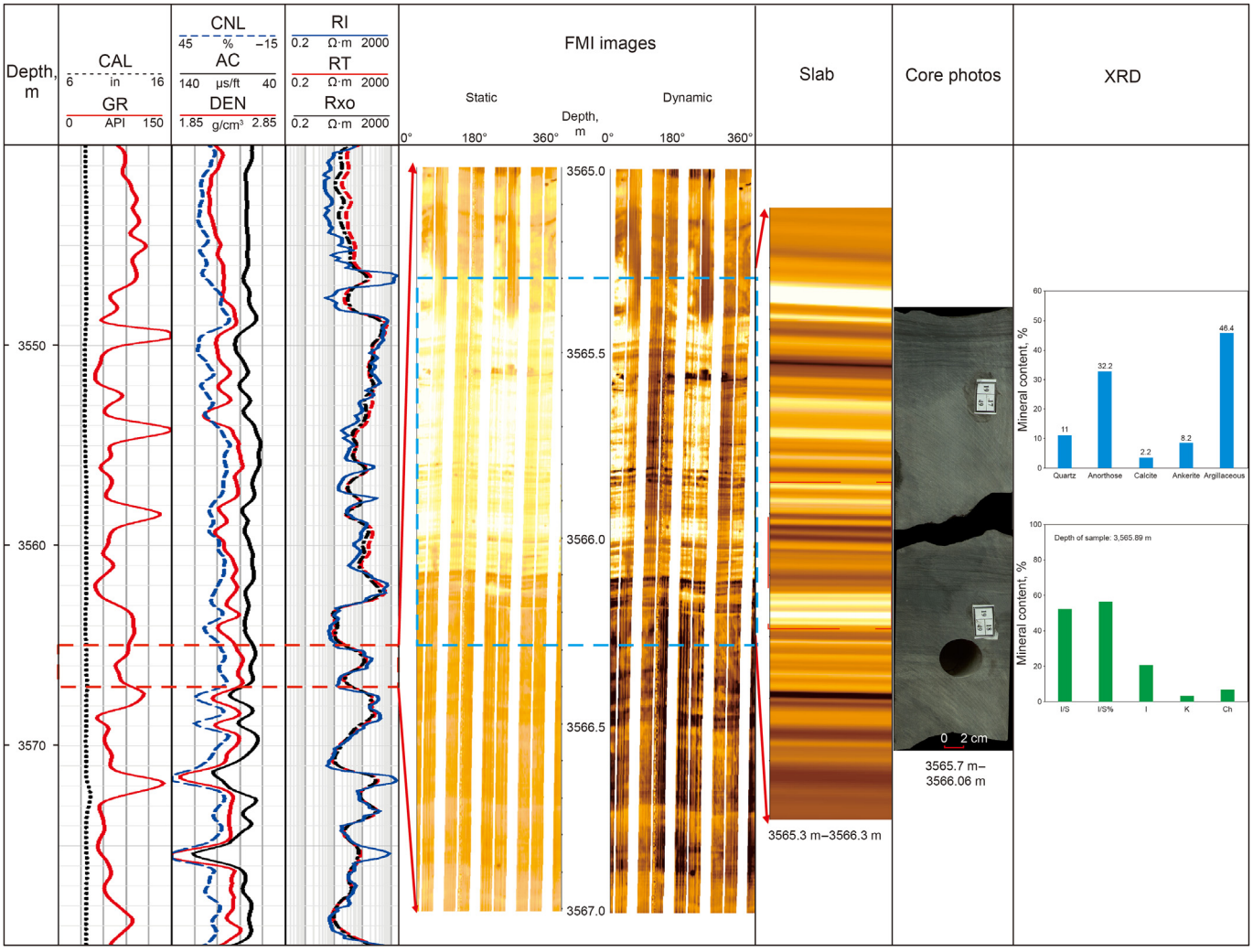

Fig. 15. Well log expression of ternary lamina (felsic, clay, organic matter) in the Lucaogou Formation in the Jimusar Sag.

The interpretation intervals A and B are typical ternary lamina combinations (felsic, clay, and organic matter), and the image logs are characterized by alternating dark, bright, and orange patterns (Fig. 17). Interval E is another representative ternary lamina structure, and the related image logs show orange-yellow and dark interbedded layers (Fig. 17).

Interval C is a representative binary lamina structure (felsic and clay), and the image logs exhibit alternating orange-yellow and dark patterns (Fig. 17), and interval G shows another type of this lamina structure (Fig. 17). Intervals D and F are typical multiple lamina structures (felsic, carbonate, organic matter, and clay), and the image logs are characterized by dark, bright, yellow, and transitional patterns (Fig. 17).

The results show that the layered rocks have the best reservoir quality (effective porosity, derived from NMR logs), whereas the massive rocks have the lowest effective porosity (Fig. 17). In laminated rocks, the results show that the higher the felsic content in the lamina structure, the better the physical properties of the reservoir. Intervals C and G have a better reservoir quality (effective porosity) than the ternary and multiple lamina combinations (Fig. 17). Furthermore, the effective porosity is medium to high (>10%) (Fig. 17).

5.2. Prediction of laminae controlled high-quality reservoirs

Reservoir quality (the amounts of porosity and permeability) is the key parameter controlling oil accumulation in fine-grained sedimentary rocks, which are self-sourced and self-reserved. The Lucaogou Formation in Jimusar has two main reservoirs: the upper sweet spot in $P_2l_2^2$ and the lower sweet spot in $P_2l_1^2$ (Liu et al., 2020). Figs. 18 and 19 show the lamina type (layered, massive, and laminated) divided by image logs and related slabs. NMR, based on investigating relaxation processes of hydrogen nuclei in the pore fluids, could provide information on a reservoir's quality (porosity, pore size distribution, fluid state, type, and permeability) (Liu et al. 2005, 2012; Daigle et al., 2014). The larger pores are associated with longer relaxation times (Mitchell and Fordham, 2014), and short T_2 relaxation times correspond to small pore throat systems (Anovitz and Cole, 2015; Meng et al., 2016). Therefore, the longer T_2 relaxation time or a tail distribution of T_2 components are relative to high reservoir quality.

In these two figs, the first track is depth, the second track shows the natural GR and CAL, the third track includes the three porosity logs (AC, CNL, and DEN), and the fourth track shows RT and Rxo log. The fifth track presents the NMR T_2 spectrum. The sixth track is the FMI image with the relevant slab in the seventh track. The eighth track is the lamina type (massive, layered, laminated), and the last track exhibits the oil test data (Figs. 18 and 19).

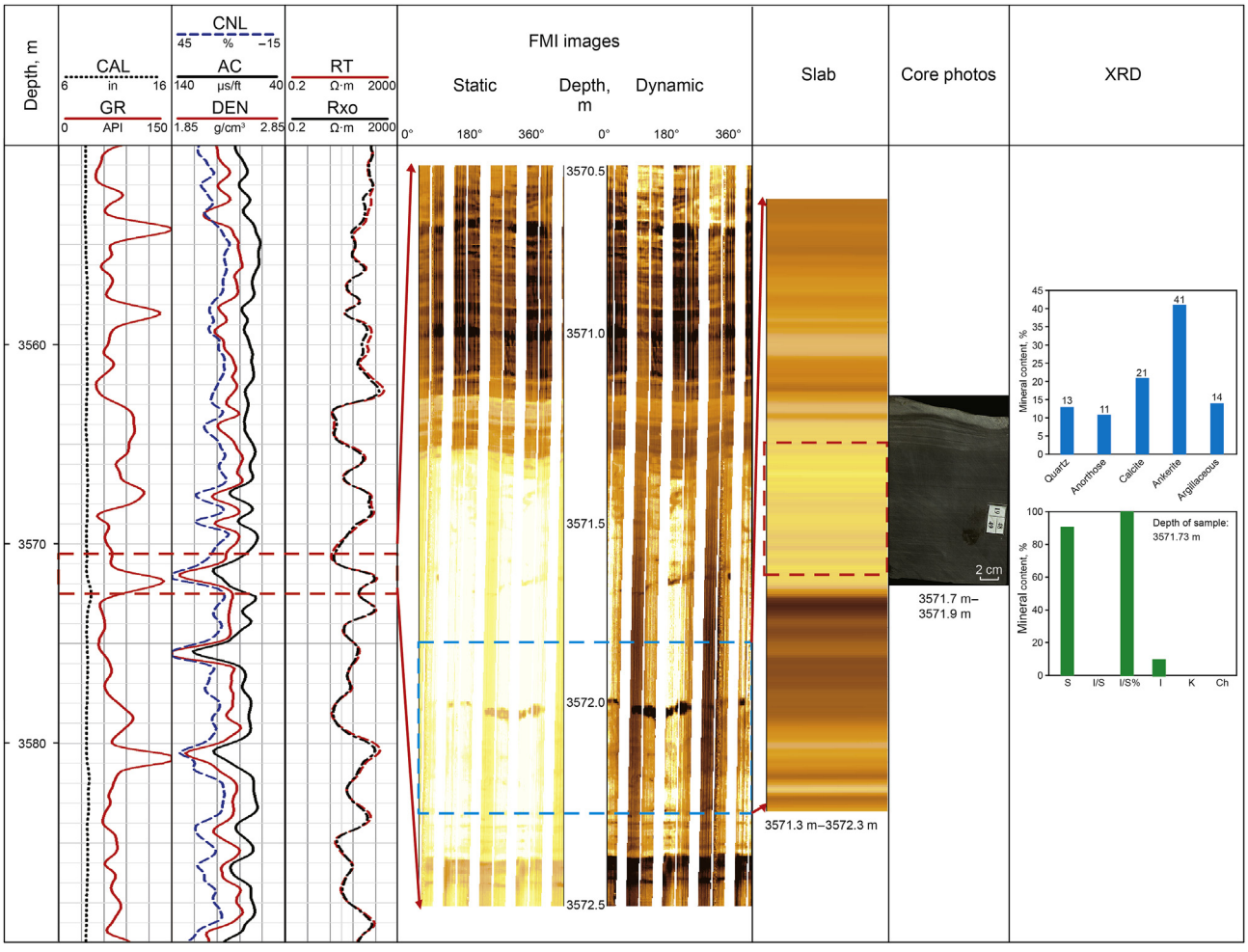

Fig. 16. Well log expression of multiple lamina (felsic, carbonate, clay, organic) in the Lucaogou Formation in the Jimusar Sag.

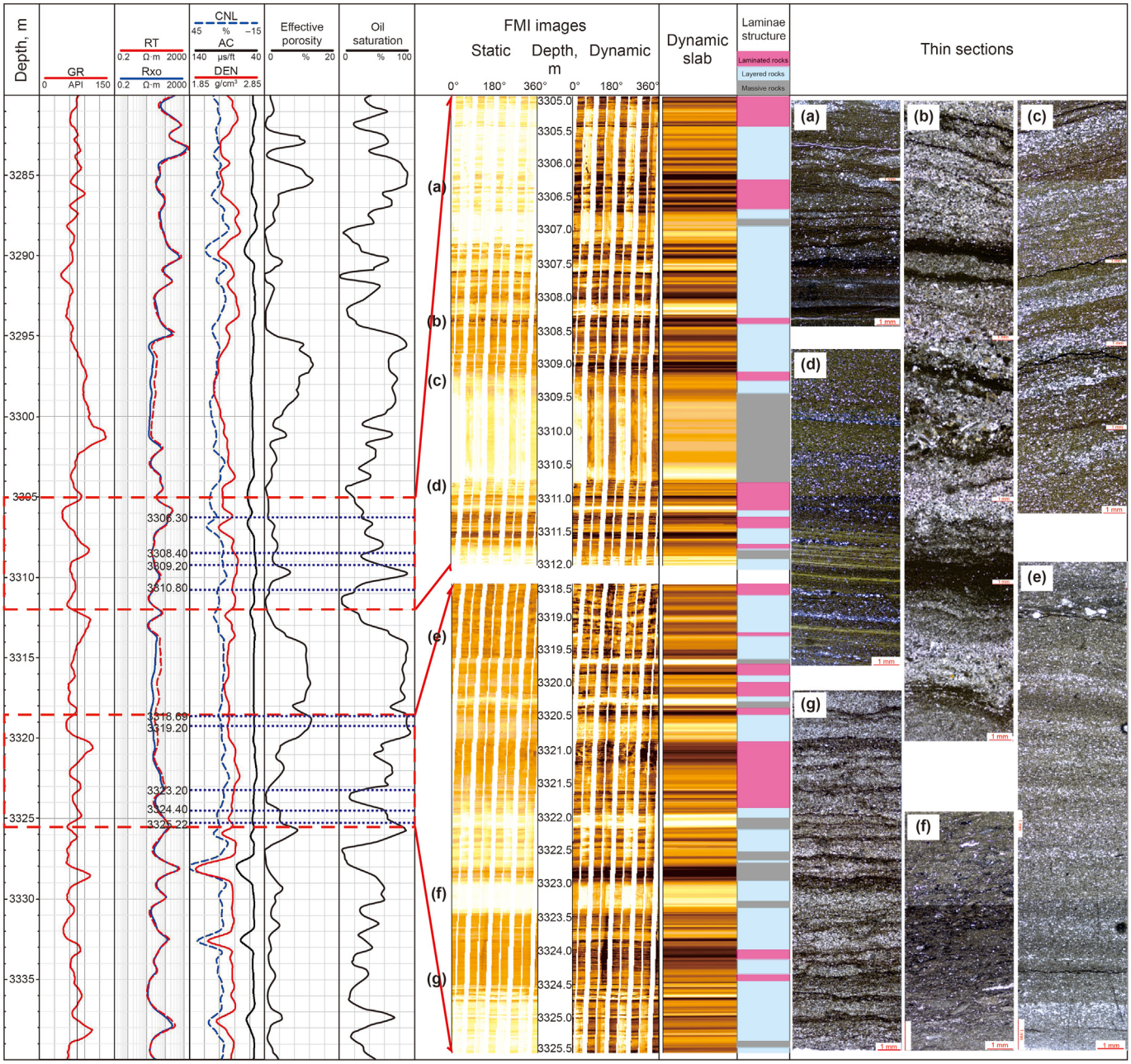

Fig. 17. Comparison of laminae recognition at various scales in J10016
(a) Ternary lamina structure (felsic, clay and organic matter), 3306.3 m. (b) Ternary lamina structure (felsic, clay and organic matter), 3308.4 m. (c) Binary lamina structure (felsic and clay), 3309.2 m. (d) Multiple lamina structure (felsic, carbonate, organic matter and clay), 3310.8 m. (e) Ternary lamina structure (felsic, clay and organic matter), 3319.2 m. (f) Multiple lamina structure (felsic, carbonate, organic matter and clay), 3323.2 m. (g) Binary lamina structure (felsic and clay), 3324.4 m.

The oil-bearing reservoirs, evidenced by oil test data, are related to the layered rocks, which have good reservoir physical properties (high effective porosity), wide T_2 distributions, and, in some cases, contain tail distributions (Figs. 18 and 19). Fig. 18 shows the upper sweet spot of Well Ji10025, characterized by layered rocks and some laminated rock interbeds. Massive rocks are rare. The layered rocks have high T_2 amplitudes and long T_2 distributions or, in some cases, have tail distributions (Fig. 18). Conversely, the massive rocks have low T_2 amplitudes, and the T_2 spectrum is unimodal. Furthermore, the laminated rocks have moderate T_2 amplitudes and no tail distributions (Fig. 18). The oil test data show that the productive intervals are associated with the layered rocks, whereas the massive rocks have poor reservoir quality (Fig. 18).

Fig. 19 displays the lower sweet spots dominated by the layered rocks. The laminated rocks are interbedded with the layered rocks, and massive rocks are rare (Fig. 19). The layered rocks are related to the intervals with high T_2 amplitudes and long T_2 distributions, indicating favorable reservoir quality and oil-bearing potential (Fig. 19). The laminated rocks are related to moderate T_2 distributions, and the T_2 amplitudes are moderate. Furthermore, the massive rocks correlate with the intervals without long T_2 components, and the T_2 distributions are narrow (Fig. 19). Therefore, the

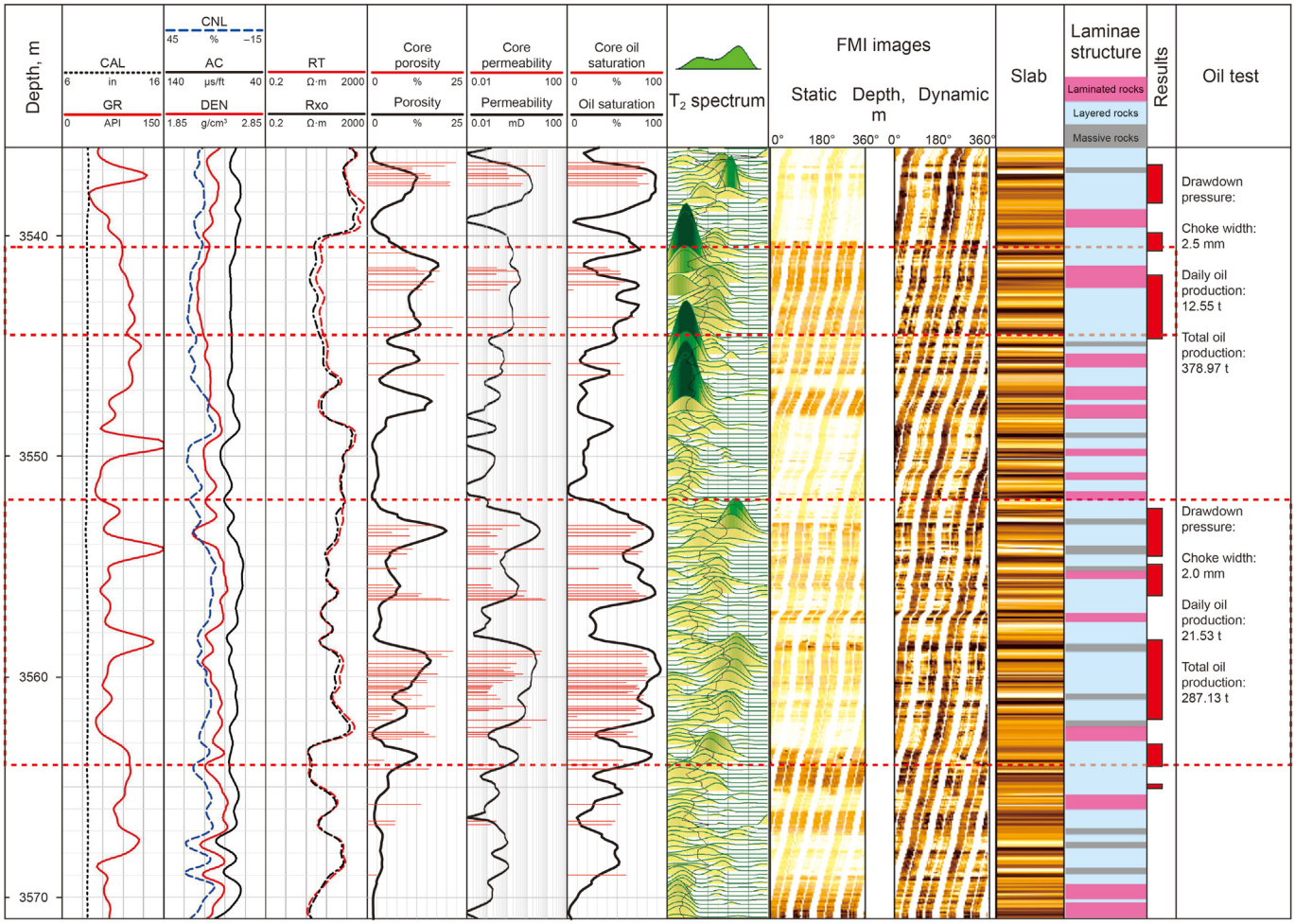

Fig. 18. Well log expression and oil test of the upper sweet spot in the Lucaogou Formation in the Jimusar Sag

T_2 distribution results show that the layered rocks have the best reservoir quality and oil-bearing potential/properties (Fig. 20), as confirmed by the oil tests (Figs. 18 and 19).

The NMR T_2 spectrum of layered rocks displays unimodal with right peak behaviors, indicating continuous pore size distribution and intergranular pores (Fig. 8) (Lai et al., 2018b). The laminated rocks have bimodal and left-skewed T_2 distributions. The high amplitudes of the right peak indicate the rareness in intergranular pores, and the abundance in the left peaks implies the abundance in small pore realms. Therefore, the laminated rocks have poorer reservoir quality and oil-bearing properties than layered rocks (Fig. 8). Massive rocks are characterized by poor reservoir quality and oil-bearing properties, as supported by the unimodal T_2 behaviors and high left peaks (Fig. 8).

Laminated and layered rocks can develop in mudstones, siltstones, and dolostones, and bedding fractures are prone to occur along the bedding planes (Vernik and Landis, 1996). Bedding fractures and structural microfractures are commonly developed, and stylolite and irregular high-angle microfractures are partly seen in the layered and laminated rocks (Zheng et al., 2019). These fractures can form favorable oil and gas migration channels, more conducive to oil and gas discharge; therefore, oil accumulates in the upper and lower layers of thin-bedded siltstone and feldspar sandstone reservoirs.

To conclude, the physical properties of the layered rocks are better than those of laminated and massive rocks. Layered rocks appear in siltstones and dolostones because they contain abundant intergranular pores, and primary pores will be favorable for intergranular and intragranular dissolution pore formation. Intergranular and intragranular pores can be evidenced by thin section observations and the NMR T_2 spectrum. The T_2 spectrum exhibits high amplitudes and right peaks. Furthermore, the connectivity of intergranular pores is high, and permeability will be high (Fig. 8e). The laminated rocks are related to siltstones (with less felsic content than the former), dolostones, and mudstones. These laminated rocks are characterized by strong heterogeneity because of rapid mineral composition changes vertically. Additionally, laminated rocks have a bimodal T_2 spectrum but are left-skewed, indicating the rareness in intergranular pores but abundance in intragranular pores.

The T_2 spectrum derived from the NMR logs revealed that a poor reservoir relates to massive rocks and a high-quality reservoir corresponds to layered rocks (Fig. 8). Massive rocks relate to mudstones and dolostones, which are source rocks with poor reservoir quality (Cao et al., 2016; Lin et al., 2021). Massive rocks contain no evident intergranular or intragranular dissolution pores, and these rocks have small pores and a narrow throat during the burial history and destructive diageneses, such as compaction and cementation. The T_2 spectrum displays unimodal and has high left peaks. Conversely, the siltstones have beddings, are characterized by layered structures, and have the best reservoir quality (Cao et al., 2016; Lin et al., 2021). In summary, layered rocks have high reservoir quality and favorable oil-

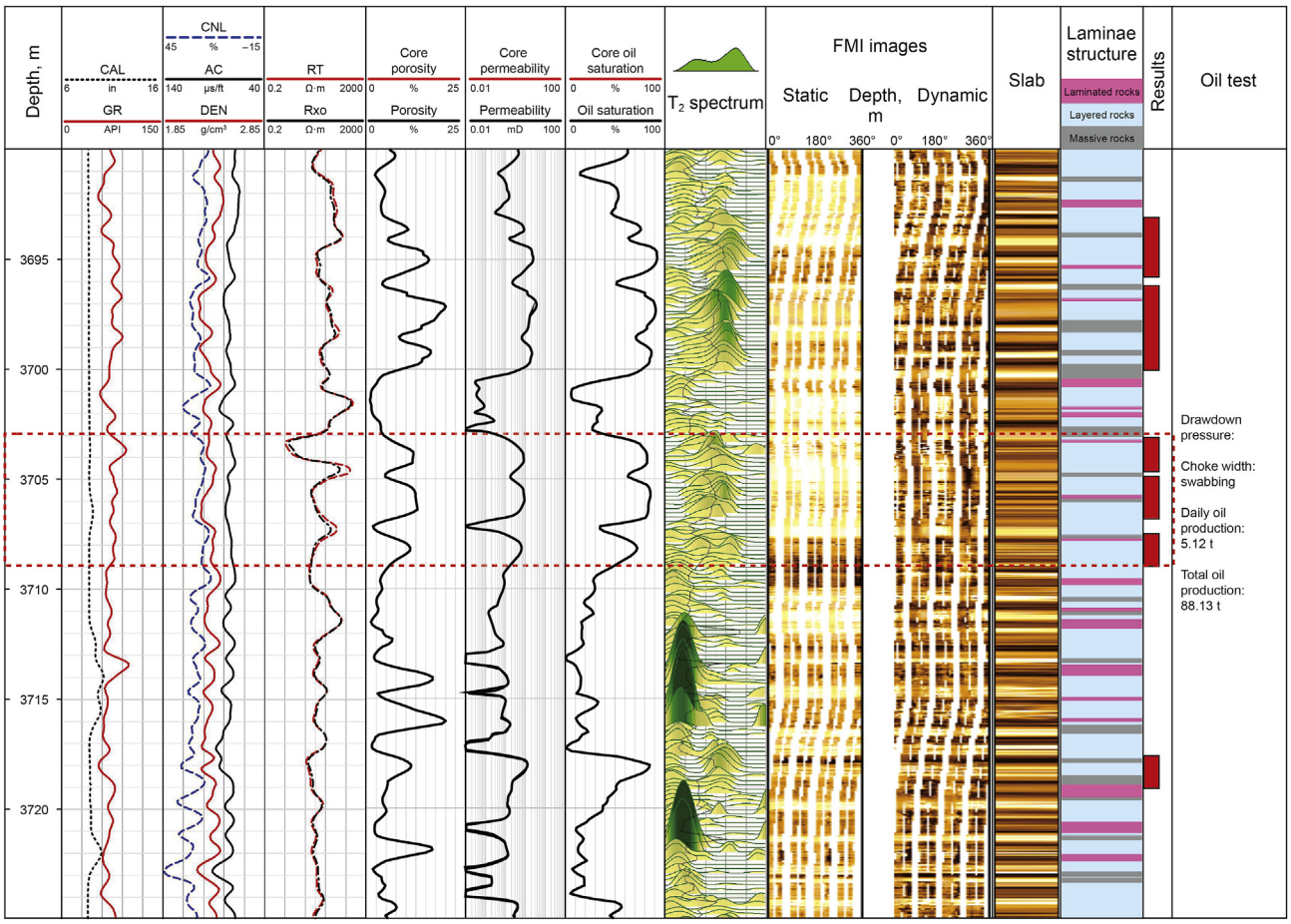

Fig. 19. Well log expression and oil test of the lower sweet spot.

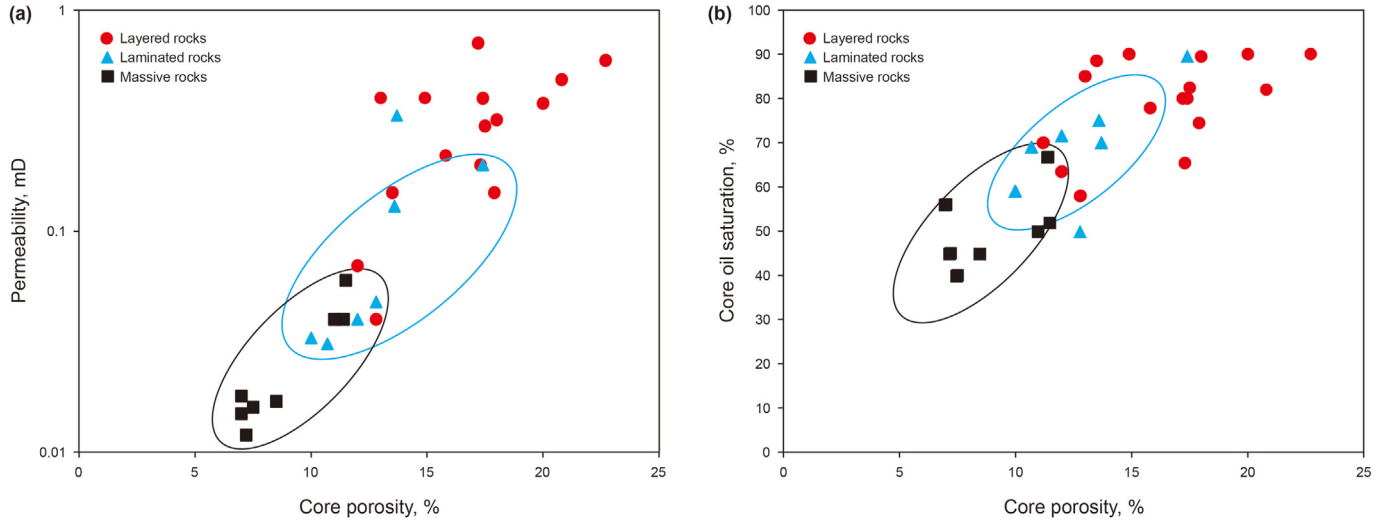

Fig. 20. Crossplots of permeability and oil saturation versus porosity for multi-scale lamina structure in the Lucaogou Formation in the Jimusar Sag (a) Cross-plot of core porosity versus core permeability. (b) Cross-plot of core porosity versus core oil saturation.

bearing properties. Conversely, massive rocks can be satisfactory source rocks with organic matter accumulation.

6. Conclusions

The lithological characteristics, pore spaces, and the lamina types of fine-grained sedimentary rocks in the Lucaogou Formation of the Jimusar Sag were studied by core and thin-section observations and well log data. The following conclusions have been reached.

Core observation exhibits three multiscale laminae combinations according to the density and thickness of individual laminae,

including massive, layered, and laminated types. Furthermore, four lamina combinations were identified according to the numerous observations of mineral components' thin section analysis. The laminated rocks can be further divided into binary (felsic and clay), ternary (felsic-carbonate-clay or felsic-clay-organic), and multiple types (felsic, clay, carbonate, or organic matter) according to the mineral superposition assemblages.

The lamina structure's scales (massive, layered, and laminated rocks) can be recognized by conventional logs, image logs, and slabs derived from image logs. Massive rocks can be differentiated from layered and laminated rocks from conventional logs combined with core and image logs. Layered and laminated rocks can be identified by the image logs and the slab of image logs. The felsic lamina is orange, the clay lamina exhibits dark, and the carbonate and organic matter laminae appear light on the slabs. The mineral superposition sequences are in millimeter scales and can only be identified by the slab.

The laminated and layered rocks are better than the massive type in reservoir properties and oil content. Furthermore, the layered rocks have the best reservoir quality. In the laminated subtype rocks, the binary type is better than the ternary and multiple types. The higher the felsic mineral content in laminated rocks, the better the reservoir's quality.

Acknowledgments

We thank PetroChina Xinjiang Oilfield Company for providing samples and data access. The authors would like to thank National Natural Science Foundation of China (Grant No. 42002133, 42072150) and Science Foundation of China University of Petroleum, Beijing (No. 2462021YXZZ003) and the Strategic Cooperation Technology Projects of CNPC and CUPB (ZLZX2020-01-06) for the financial supports and permissions to publish this paper. We also acknowledge the diligent work of the reviewers, which helps improve the manuscript.

References

Abuamarah, B.A., Nabawy, B.S., Shehata, A.M., et al., 2019. Integrated geological and petrophysical characterization of oligocene deep marine unconventional poor to tight sandstone gas reservoir. Mar. Petrol. Geol. 109, 868–885. https://doi.org/10.1016/j.marpetgeo.2019.06.037.

Allen, M.B., Engör, A.M.C., 1995. Natal'In BA. Turfan and Alakol basins as late permian to early Triassic extensional structures in a sinistral shear zone in the Altaid orogenic collage, central Asia. J. Geol. Soc. 152 (2), 327–338. https://doi.org/10.1144/gsjgs.152.2.0327.

Altawati, F., Emadi, H., Pathak, S., 2021. Improving oil recovery of Eagle Ford shale samples using cryogenic and cyclic gas injection methods-an experimental study. Fuel 302, 121170. https://doi.org/10.1016/j.fuel.2021.121170.

Anderson, R.Y., 1996. Seasonal sedimentation: a framework for reconstructing climatic and environmental change. Geol. Soc. Lond. Spec. Publ. 116 (1), 1–15. https://doi.org/10.1144/GSL.SP.1996.116.01.02.

Anovitz, L.M., Cole, D.R., 2015. Characterization and analysis of porosity and pore structures. Rev. Mineral. Geochem. 80 (1), 61–164. https://doi.org/10.2138/rmg.2015.80.04.

Aplin, A.C., Macquaker, J.S.H., 2011. Mudstone diversity: implications for source, seal, and reservoir properties in petroleum systems. AAPG (Am. Assoc. Pet. Geol.) Bull. 95 (12), 2031–2059. https://doi.org/10.1306/03281110162.

Bai, L.H., Liu, B., Du, Y.J., et al., 2022. Distribution characteristics and oil mobility thresholds in lacustrine shale reservoir: insights from N_2 adsorption experiments on samples prior to and following hydrocarbon extraction. Petrol. Sci. 19 (2), 486–497. https://doi.org/10.1016/j.petsci.2021.10.018.

Bennett, R.H., Bryant, W.R., Hulbert, M.H., 1991. Microstructure of Fine-Grained Sediments: from Mud to Shale. Springer Science & Business Media, pp. 108–124. https://doi.org/10.1007/978-1-4612-4428-8.

Bize, E., Tisi, A., Laronga, R., et al., 2015. Virtual core: state-of-the-art wireline technologies to provide a viable substitute for whole conventional coring. Offshore Technol. Conf. https://doi.org/10.4043/26206-MS.

Cai, Q.S., Hu, M.Y., Zhang, B.M., et al., 2022. Source of silica and its implications for organic matter enrichment in the Upper Ordovician-Lower Silurian black shale in western Hubei Province, China: insights from geochemical and petrological analysis. Petrol. Sci. 19 (1), 74–90. https://doi.org/10.1016/j.petsci.2021.10.012.

Cao, J., Xia, L.W., Wang, T.T., et al., 2020. An alkaline lake in the Late Paleozoic Ice Age (LPIA): a review and new insights into paleoenvironment and petroleum geology. Earth Sci. Rev. 202, 103091. https://doi.org/10.1016/j.earscirev.2020.103091.

Cao, Z., Liu, G.D., Kong, Y.H., et al., 2016. Lacustrine tight oil accumulation characteristics: Permian Lucaogou Formation in Jimusaer sag, Junggar Basin. Int. J. Coal Geol. 135, 37–51. https://doi.org/10.1016/j.coal.2015.11.004.

Cao, Z., Liu, G., Zhan, H., et al., 2017. Geological roles of the siltstones in tight oil play. Mar. Petrol. Geol. 83, 333–344. https://doi.org/10.1016/j.marpetgeo.2017.02.020.

Chen, S.Y., Zhang, S., Liu, H.M., et al., 2017. Discussion on mixing of fine-grained sediments in lacustrine deep water. J. Paleogeogr. 19 (2), 271–283. https://doi.org/10.7605/gdlxb.2017.02.021.

Curtis, J.B., 2002. Fractured shale-gas systems. AAPG Bull. 86 (11), 1921–1938. https://doi.org/10.1306/61EEDDBE-173E-11D7-8645000102C1865D.

Daigle, H., Thomas, B., Rowe, H., et al., 2014. Nuclear magnetic resonance characterization of shallow marine sediments from the Nankai trough, integrated ocean drilling program expedition 333. J. Geophys. Res. Solid Earth 119, 2631–2650. https://doi.org/10.1002/2013JB010784.

Davies, D.K., Bryant, W.R., Vessell, R.K., et al., 1991. Porosities, Permeabilities, and Microfabrics of Devonian Shales. Springer, New York, pp. 109–119. https://doi.org/10.1007/978-1-4612-4428-8_10.

El Sharawy, M.S., Nabawy, B.S., 2016. Geological and petrophysical Characterization of the lower Senonian Matulla Formation in southern and central Gulf of Suez, Egypt. Arabian J. Sci. Eng. 41 (1), 281–300. https://doi.org/10.1007/s13369-015-1806-7.

English, J.M., Laubach, S.E., 2017. Opening-mode fracture systems: insights from recent fluid inclusion microthermometry studies of crack-seal fracture cements. Geol. Soc. Lond. Spec. Publ. 458 (1), 257–272. https://doi.org/10.1144/SP458.1.

Feng, Q.F., Xiao, Y.X., Hou, X.L., et al., 2021. Logging identification method of depositional facies in Sinian Dengying formation of the Sichuan basin. Petrol. Sci. 18 (4), 1086–1096. https://doi.org/10.1016/j.petsci.2020.10.002.

Folkestad, A., Veselovsky, Z., Roberts, P., 2012. Utilising borehole image logs to interpret delta to estuarine system: a case study of the subsurface Lower Jurassic Cook Formation in the Norwegian northern North Sea. Mar. Petrol. Geol. 29 (1), 255–275. https://doi.org/10.1016/j.marpetgeo.2011.07.008.

Gale, J.F., Laubach, S.E., Olson, J.E., et al., 2014. Natural fractures in shale: a review and new observations Natural fractures in shale: a review and new observations. AAPG (Am. Assoc. Pet. Geol.) Bull. 98 (11), 2165–2216. https://doi.org/10.1306/08121413151.

Gale, J.F., Reed, R.M., Holder, J., 2007. Natural fractures in the Barnett Shale and their importance for hydraulic fracture treatments. AAPG (Am. Assoc. Pet. Geol.) Bull. 91 (4), 603–622. https://doi.org/10.1306/11010606061.

Gao, G., Zhang, W.W., Xiang, B.L., et al., 2016. Geochemistry characteristics and hydrocarbon-generating potential of lacustrine source rock in Lucaogou Formation of the Jimusaer sag, Junggar Basin. J. Petrol. Sci. Eng. 145, 168–182. https://doi.org/10.1016/j.petrol.2016.03.023.

Ghanizadeh, A., Clarkson, C.R., Aquino, S., et al., 2015. Petrophysical and geomechanical characteristics of Canadian tight oil and liquid-rich gas reservoirs: I. Pore network and permeability characterization. Fuel 153, 664–681. https://doi.org/10.1016/j.fuel.2015.03.020.

Golsanami, N., Kadkhodaie-Ilkhchi, A., Sharghi, Y., et al., 2014. Estimating NMR T_2 distribution data from well log data with the use of a committee machine approach: a case study from the Asmari formation in the Zagros basin, Iran. J. Petrol. Sci. Eng. 114, 38–51. https://doi.org/10.1016/j.petrol.2013.12.003.

Guan, M., Liu, X., Jin, Z., et al., 2020. The heterogeneity of pore structure in lacustrine shales: insights from multifractal analysis using N_2 adsorption and mercury intrusion. Mar. Petrol. Geol. 114, 104150. https://doi.org/10.1016/j.marpetgeo.2019.104150.

He, D., Li, D., Fan, C., et al., 2013. Geochronology, geochemistry and tectonostratigraphy of Carboniferous strata of the deepest well Moshen-1 in the Junggar Basin, northwest China: insights into the continental growth of central Asia. Gondwana Res. 24 (2), 560–577. https://doi.org/10.1016/j.gr.2012.10.015.

Heng, S., Li, X., Liu, X., et al., 2020. Experimental study on the mechanical properties of bedding planes in shale. J. Nat. Gas Sci. Eng. 76, 103161. https://doi.org/10.1016/j.jngse.2020.103161.

Hill, R.J., Zhang, E., Katz, B.J., et al., 2007. Modeling of gas generation from the Barnett shale, fort Worth basin, Texas. AAPG (Am. Assoc. Pet. Geol.) Bull. 91 (4), 501–521. https://doi.org/10.1306/12060606063.

Hooker, J.N., Larson, T.E., Eakin, A., et al., 2015. Fracturing and fluid flow in a subdécollement sandstone; or, a leak in the basement. J. Geol. Soc. Lond. 172 (4), 428–442. https://doi.org/10.1144/jgs2014-128.

Hurley, N., Zhang, T., 2011. Method to generate fullbore images using borehole images and multi-point statistics. SPE Reserv. Eval. Eng. 14 (2), 204–214. https://doi.org/10.2118/120671-PA.

Khoshbakht, F., Azizzadeh, M., Memarian, H., et al., 2012. Comparison of electrical image log with core in a fractured carbonate reservoir. J. Petrol. Sci. Eng. 86, 289–296. https://doi.org/10.1016/j.petrol.2012.03.007.

Krumbein, W.C., 1947. Shales and their environmental significance. J. Sediment. Petrol. 17 (3), 101–108. https://doi.org/10.1306/D42692BF-2B26-11D7-8648000102C1865D.

Kuang, L.C., Gao, G., Xiang, B., et al., 2014. Lowest limit of organic carbon content in effective source rocks from Lucaogou Formation in Jimusar Sag. Petrol. Geol. Exp. 36 (2), 224–229. https://doi.org/10.11781/sysydz201402224.

Kuang, L.C., Tang, Y., Lei, D.W., et al., 2012. Formation conditions and exploration potential of tight oil in the Permian saline lacustrine dolomitic rock, Junggar

Basin, NW China. Petrol. Explor. Dev. 39 (6), 700–711. https://doi.org/10.1016/S1876-3804(12)60095-0.
Kumar, A., Laronga, R., Kherroubi, J., et al., 2014. Visualizing Borehole Images in a Slabbed-Core Format. EAGE 1st Borehole Geology Workshop, Dubai, UAE. https://doi.org/10.3997/2214-4609.20142331.
Lagraba, P., Hansen, S.M., Spalburg, M., et al., 2010. Borehole image tool design, value of information, and tool selection. In: Pöppelreiter, M., García-Carballido, C., Kraaijveld, M. (Eds.), Dipmeter and Borehole Image Log Technology, vol. 92. AAPG Memoir, pp. 15–38. https://doi.org/10.1306/13181275M923403.
Lai, J., Chen, K.J., Xin, Y., et al., 2020. Fracture characterization and detection in the deep Cambrian dolostones in the Tarim Basin, China: insights from borehole image and sonic logs. J. Petrol. Sci. Eng. 196, 107659. https://doi.org/10.1016/j.petrol.2020.107659.
Lai, J., Liu, B., Li, H., et al., 2022a. Bedding parallel fractures in fine-grained sedimentary rocks: recognition, formation mechanisms, and prediction using well log. Petrol. Sci. 19 (2), 554–569. https://doi.org/10.1016/j.petsci.2021.10.017.
Lai, J., Liu, S., Xin, Y., et al., 2021. Geological-petrophysical insights in the deep Cambrian dolostone reservoirs in Tarim Basin, China. AAPG Bull. 105 (11), 2263–2296. https://doi.org/10.1306/03122119135.
Lai, J., Wang, G., Fan, Q., et al., 2022b. Geophysical well log evaluation in the era of unconventional hydrocarbon resources: A review on current status and prospects. Surv. Geophys. 43, 913–957. https://doi.org/10.1007/s10712-022-09705-4.
Lai, J., Wang, G., Huang, L., et al., 2015. Brittleness index estimation in a tight shaly sandstone reservoir using well logs. J. Nat. Gas Sci. Eng. 27, 1536–1545. https://doi.org/10.1016/j.jngse.2015.10.020.
Lai, J., Wang, G., Ran, Y., et al., 2016. Impact of diagenesis on the reservoir quality of tight oil sandstones: the case of Upper Triassic Yanchang Formation Chang 7 oil layers in Ordos Basin, China. J. Petrol. Sci. Eng. 145, 54–65. https://doi.org/10.1016/j.petrol.2016.03.009.
Lai, J., Wang, G., Wang, S., et al., 2018a. A review on the applications of image logs in structural analysis and sedimentary characterization. Mar. Petrol. Geol. 95, 139–166. https://doi.org/10.1016/j.marpetgeo.2018.04.020.
Lai, J., Wang, G., Wang, Z., et al., 2018b. A review on pore structure characterization in tight sandstones. Earth Sci. Rev. 177, 436–457. https://doi.org/10.1016/j.earscirev.2017.12.003.
Lei, Y.H., Luo, X.L., Wang, X., et al., 2015. Characteristics of silty laminae in Zhangjiatan Shale of southeastern Ordos Basin, China: implications for shale gas formation. AAPG (Am. Assoc. Pet. Geol.) Bull. 99 (4), 661–687. https://doi.org/10.1306/09301414059.
Li, L.H., Huang, B.X., Li, Y.Y., et al., 2018. Multi-scale modeling of shale laminaes and fracture networks in the Yanchang formation, southern Ordos basin, China. Eng. Geol. 243, 231–240. https://doi.org/10.1016/j.enggeo.2018.07.010.
Li, L.H., Huang, B.X., Tan, Y.F., et al., 2017. 2017. Geometric heterogeneity of continental shale in the Yanchang formation, southern Ordos basin, China. Sci. Rep. 7 (1), 1–12. https://doi.org/10.1038/s41598-017-05144-z.
Li, J., Wang, M., Lu, S., et al., 2020. A new method for predicting sweet spots of shale oil using conventional well logs. Mar. Petrol. Geol. 113, 104097. https://doi.org/10.1016/j.marpetgeo.2019.104097.
Li, J.H., Li, B.B., Cheng, Q.Y., et al., 2021. Characterization of the fracture compressibility and its permeability for shale under the effects of proppant embedment and compaction: a preliminary study. Petrol. Sci. https://doi.org/10.1016/j.petsci.2021.12.021.
Lin, M., Xi, K., Cao, Y., et al., 2021. Petrographic features and diagenetic alteration in the shale strata of the Permian Lucaogou Formation, Jimusar sag, Junggar Basin. J. Petrol. Sci. Eng. 203, 108684. https://doi.org/10.1016/j.petrol.2021.108684.
Liu, B., Wang, H., Fu, X., et al., 2019a. Lithofacies and depositional setting of a highly prospective lacustrine shale oil succession from the Upper Cretaceous Qingshankou Formation in the Gulong sag, northern Songliao Basin, northeast China. AAPG (Am. Assoc. Pet. Geol.) Bull. 103 (2), 405–432. https://doi.org/10.1306/08031817416.
Liu, C., Liu, K., Wang, X., et al., 2019b. Chemo-sedimentary facies analysis of fine-grained sediment formations: an example from the Lucaogou Fm in the Jimusaer sag, Junggar Basin, NW China. Mar. Petrol. Geol. 110, 388–402. https://doi.org/10.1016/j.marpetgeo.2019.06.043.
Liu, G.H., Liu, B., Huang, Z.L., et al., 2018. Hydrocarbon distribution pattern and logging identification in lacustrine fine-grained sedimentary rocks of the Permian Lucaogou Formation from the Santanghu basin. Fuel 222, 207–231. https://doi.org/10.1016/j.fuel.2018.02.123.
Liu, T.Y., Jun, Y., Jie, Y., 2012. Theoretical mechanism and application of Sphere-Cylinder model in NMR for oil-water porous media. Pure Appl. Geophys. 169 (7), 1257–1267. https://doi.org/10.1007/s00024-011-0395-y.
Liu, T.Y., Ma, Z.T., Lv, H.Z., 2005. Integrating MDT, NMR log and conventional logs for one-well evaluation. J. Petrol. Sci. Eng. 46 (1–2), 73–80. https://doi.org/10.1016/j.petrol.2004.09.001.
Liu, X.P., Lai, J., Fan, X.C., et al., 2020. Insights in the pore structure, fluid mobility and oiliness in oil shales of Paleogene Funing Formation in Subei Basin, China. Mar. Petrol. Geol. 114, 104228. https://doi.org/10.1016/j.marpetgeo.2020.104228.
Liu, Y.Y., Ma, X.H., Zhang, X.W., et al., 2021. A deep-learning-based prediction method of the estimated ultimate recovery (EUR) of shale gas wells. Petrol. Sci. 18 (5), 1450–1464. https://doi.org/10.1016/j.petsci.2021.08.007.
Loucks, R.G., Reed, R.M., Ruppel, S.C., et al., 2009. Morphology, genesis, and distribution of nanometer-scale pores in siliceous mudstones of the Mississippian Barnett Shale. J. Sediment. Res. 79 (12), 848–861. https://doi.org/10.2110/jsr.2009.092.
Lu, X.C., Shi, J.A., Zhang, S.C., et al., 2015. The origin and formation model of Permian dolostones on the northwestern margin of Junggar Basin, China. J. Asian Earth Sci. 105, 456–467. https://doi.org/10.1016/j.jseaes.2015.02.024.
Ma, C., Wang, J., Pan, X.H., et al., 2020. Origin and significance of “sweet spots” of analcites in shale oil reservoirs in Permian Lucaogou Formation, Jimsar sag, Junggar Basin. Petrol. Geol. Exp. 42 (4), 596–603. https://doi.org/10.11781/sysydz202004596.
Ma, L., Dowey, P.J., Rutter, E., et al., 2019. A novel upscaling procedure for characterizing heterogeneous shale porosity from nanometer-to millimetre-scale in 3D. Energy 181, 1285–1297. https://doi.org/10.1016/j.energy.2019.06.011.
Meng, M., Ge, H., Ji, W., et al., 2016. Research on the auto-removal mechanism of shale aqueous phase trapping using low field nuclear magnetic resonance technique. J. Petrol. Sci. Eng. 137, 63–73. https://doi.org/10.1016/j.petrol.2015.11.012.
Mitchell, J., Fordham, E.J., 2014. Contributed Review: nuclear magnetic resonance core analysis at 0.3 T. Rev. Sci. Instrum. 85 (11), 111502. https://doi.org/10.1063/1.4902093.
Moreau, J., Joubert, J.B., 2016. Glacial sedimentology interpretation from borehole image log: example from the Late Ordovician deposits, Murzuq Basin (Libya). Interpretation 4 (2), B1–B16. https://doi.org/10.1190/INT-2015-0161.1.
Muniz, M.C., Bosence, D.W.J., 2015. Pre-salt microbialites from the campos basin (offshore Brazil): image log facies, facies model and cyclicity in lacustrine carbonates. Geol. Soc. Lond. Spec. Publ. 418 (1), 221–242. https://doi.org/10.1144/SP418.10.
Nabawy, B.S., El Sharawy, M.S., 2015. Hydrocarbon potential, structural setting and depositional environments of Hammam Faraun member of the Belayim formation, southern Gulf of Suez, Egypt. J. Afr. Earth Sci. 112, 93–110. https://doi.org/10.1016/j.jafrearsci.2015.09.010.
Nabawy, B.S., Elgendy, N.T.H., Gazia, M.T., 2020. Mineralogic and diagenetic Controls on reservoir quality of paleozoic sandstones, Gebel El-Zeit, North Eastern Desert, Egypt. Nat. Resour. Res. 29 (2), 1215–1238. https://doi.org/10.1007/s11053-019-09487-4.
Pang, X.J., Wang, G.W., Kuang, L.C., et al., 2022. Insights into the pore structure and oil mobility in fine-grained sedimentary rocks: the Lucaogou Formation in Jimusar Sag, Junggar Basin, China. Mar. Petrol. Geol. 137, 105492. https://doi.org/10.1016/j.marpetgeo.2021.105492.
Qi, X., Wu, X., Tang, Y., et al., 2013. Minerogenetic characteristics and resources potential of Permian oil shale in the northern slope of Bogda Mountain in Xinjiang. Chin. J. Geol. 48 (4), 1271–1285. https://doi.org/10.3969/j.issn.0563-5020.2013.04.022 (in Chinese).
Qiu, Z., Tao, H.F., Zou, C.N., et al., 2016. Lithofacies and organic geochemistry of the middle Permian Lucaogou Formation in the Jimusar sag of the Junggar Basin, NW China. Petrol. Explor. Dev. 140, 97–107. https://doi.org/10.1016/j.petrol.2016.01.014.
Rajabi, M., Sherkati, S., Bohloli, B., et al., 2010. Subsurface fracture analysis and determination of in-situ stress direction using FMI logs: an example from the Santonian carbonates (Ilam Formation) in the Abadan Plain, Iran. Tectonophysics 492 (1–4), 192–200. https://doi.org/10.1016/j.tecto.2010.06.014.
Rickman, R., Mullen, M.J., Petre, J.E., et al., 2008. A Practical Use of Shale Petrophysics for Stimulation Design Optimization: All Shale Plays Are Not Clones of the Barnett Shale. SPE Annual Technical Conference and Exhibition. Society of Petroleum Engineers. https://doi.org/10.2118/115258-MS.
Saidian, M., Prasad, M., 2015. Effect of mineralogy on nuclear magnetic resonance surface relaxivity: a case study of Middle Bakken and Three Forks formations. Fuel 161, 197–206. https://doi.org/10.1016/j.fuel.2015.08.014.
Schieber, J., 1991. Sedimentary Structures: Textures and Depositional Settings of Shales from the Lower Belt Supergroup, Mid-proterozoic, Montana, USA. Microstructure of Fine-Grained Sediments. Springer, New York, NY, pp. 101–108. https://doi.org/10.1007/978-1-4612-4428-8_9.
Serra, O., 1989. Formation Microscanner Image Interpretation. Schlumberger Educational Services, Houston Texas, p. 117.
Shi, Z.S., Qiu, Z., 2021. Main bedding types of marine fine-grained sediments and their significance for oil and gas exploration and development. Acta Sedimentol. Sin. 39 (1), 181–196. https://doi.org/10.14027/j.issn.1000-0550.2020.097.
Sun, C., Zheng, H., Liu, W.D., et al., 2020. Numerical simulation analysis of vertical propagation of hydraulic fracture in bedding plane. Eng. Fract. Mech. 232, 107056. https://doi.org/10.1016/j.engfracmech.2020.107056.
Sun, C.H., James, McClure, Berg, Steffen, et al., 2022. Universal description of wetting on multiscale surfaces using integral geometry. J. Colloid Interface Sci. 608, 2330–2338. https://doi.org/10.1016/j.jcis.2021.10.152.
Tang, X., Jiang, S., Jiang, Z., et al., 2019. Heterogeneity of Paleozoic Wufeng-Longmaxi formation shale and its effects on the shale gas accumulation in the Upper Yangtze Region, China. Fuel 239, 387–402. https://doi.org/10.1016/j.fuel.2018.11.022.
Vernik, L., Landis, C., 1996. Elastic anisotropy of source rocks: implications for hydrocarbon generation and primary Migration1. AAPG Bull. 80 (4), 531–544. https://doi.org/10.1306/64ED8836-1724-11D7-8645000102C1865D.
Wang, C., Zhang, B., Hu, Q., et al., 2019. Laminae characteristics and influence on shale gas reservoir quality of lower Silurian Longmaxi Formation in the Jiaoshiba area of the Sichuan Basin, China. Mar. Petrol. Geol. 109, 839–851. https://doi.org/10.1016/j.marpetgeo.2019.06.022.
Wang, S., Wang, G., Huang, L., et al., 2021. Logging evaluation of lamina structure and reservoir quality in shale oil reservoir of Fengcheng Formation in Mahu Sag,

China. Mar. Petrol. Geol. 133, 105299. https://doi.org/10.1016/j.marpetgeo.2021.105299.
Wang, Y.C., Cao, J., Tao, K.Y., et al., 2020. Reevaluating the source and accumulation of tight oil in the middle Permian Lucaogou Formation of the Junggar Basin, China. Mar. Petrol. Geol. 117, 104384. https://doi.org/10.1016/j.marpetgeo.2020.104384.
Wu, S.T., Zhai, X.F., Yang, Z., et al., 2019. Characterization of fracture formation in organic-rich shales-An experimental and real time study of the Permian Lucaogou Formation, Junggar Basin, northwestern China. Mar. Petrol. Geol. 107, 397–406. https://doi.org/10.1016/j.marpetgeo.2019.05.036.
Xi, K.L., Cao, Y.C., Lin, M.R., et al., 2020. Laminae combination and shale oil enrichment patterns of Chang 73 sub-member organic-rich shales in the Triassic Yanchang Formation, Ordos Basin, NW China. Petrol. Explor. Dev. 47 (6), 1342–1353. https://doi.org/10.1016/S1876-3804(20)60142-8.
Xi, K.L., Cao, Y.C., Zhu, R.K., et al., 2015. Rock type sand characteristics of tight oil reservoir in Permian Lucaogou Formation, Jimsar sag. Acta Petrol. Sin. 36 (12), 1495–1507. https://doi.org/10.7623/syxb201512004.
Xiao, W., Han, C., Yuan, C., et al., 2008. Middle Cambrian to Permian subduction-related accretionary orogenesis of Northern Xinjiang, NW China: implications for the tectonic evolution of central Asia. J. Asian Earth Sci. 32 (2–4), 102–117. https://doi.org/10.1016/j.jseaes.2007.10.008.
Xiong, Z.H., Cao, Y.C., Wang, G.M., et al., 2019. Influence of laminar structure differences on the fracability of lacustrine fine-grained sedimentary rocks. Acta Pet. Sin. 40 (1), 74–85. https://doi.org/10.7623/syxb201901006.
Xu, C., Gehenn, J.M., Zhao, D., et al., 2015. The fluvial and lacustrine sedimentary systems and stratigraphic correlation in the Upper Triassic Xujiahe Formation in Sichuan Basin, China. AAPG (Am. Assoc. Pet. Geol.) Bull. 99 (11), 2023–2041. https://doi.org/10.1306/07061514236.
Yang, Z., Zou, C.N., Wu, S.T., et al., 2019. Formation, distribution and resource potential of the "sweet areas (sections)" of continental shale oil in China. Mar. Petrol. Geol. 102, 48–60. https://doi.org/10.1016/j.marpetgeo.2018.11.049.
Yawar, Z., Schieber, J., 2017. On the origin of silt laminaee in laminated shales. Sediment. Geol. 360, 22–34. https://doi.org/10.1016/j.sedgeo.2017.09.001.
Yuan, X., Lin, S.H., Liu, Q., et al., 2015. Lacustrine fine-grained sedimentary features and organic-rich shale distribution pattern: a case study of Chang 7 Member of Triassic Yanchang Formation in Ordos Basin, NW China. Petrol. Explor. Dev. 42 (1), 37–47. https://doi.org/10.1016/S1876-3804(15)60004-0.
Zeng, L., Li, X., 2009. Fractures in sandstone reservoirs with ultra-low permeability: a case study of the upper Triassic Yanchang Formation in the Ordos basin, China. AAPG (Am. Assoc. Pet. Geol.) Bull. 93 (4), 461–477. https://doi.org/10.1306/09240808047.
Zhang, C., Zhu, D.Y., Luo, Q., et al., 2017. Major factors controlling fracture development in the Middle Permian Lucaogou Formation tight oil reservoir, Junggar Basin, NW China. J. Asian Earth Sci. 146, 279–295. https://doi.org/10.1016/j.jseaes.2017.04.032.
Zhang, P., Lu, S., Li, J., et al., 2018. Petrophysical characterization of oil-bearing shales by low-field nuclear magnetic resonance (NMR). Mar. Petrol. Geol. 89, 775–785. https://doi.org/10.1016/j.marpetgeo.2017.11.015.
Zhang, S.M., Cao, Y.C., Liu, K.Y., et al., 2019. Characterization of lacustrine mixed fine-grained sedimentary rocks using coupled chemostratigraphic-petrographic analysis: a case study from a tight oil reservoir in the Jimusar Sag, Junggar Basin. Mar. Petrol. Geol. 99, 453–472. https://doi.org/10.1016/j.marpetgeo.2018.10.039.
Zhao, K., Du, X., Lu, Y., et al., 2019. Are light-dark coupled laminae in lacustrine shale seasonally controlled? A case study using astronomical tuning from 42.2 to 45.4 Ma in the Dongying Depression, Bohai Bay Basin, eastern China. Palaeogeogr. Palaeoclimatol. Palaeoecol. 528, 35–49. https://doi.org/10.1016/j.palaeo.2019.04.034.
Zhao, S.J., Li, S.Z., Liu, X., et al., 2014. Intracontinental orogenic transition: insights from structures of the eastern Junggar Basin between the Altay and Tianshan orogens. J. Asian Earth Sci. 88, 137–148. https://doi.org/10.1016/j.jseaes.2014.03.008.
Zheng, D., Wang, W., Rez, Z., 2019. Integrated pore-scale characterization of mercury injection/imbibition and isothermal adsorption/desorption experiments using dendroidal model for shales. J. Petrol. Sci. Eng. 178, 751–765. https://doi.org/10.1016/j.petrol.2019.03.054.
Zhu, X.M., 2021. Sedimentology. Petroleum Industry Press, Beijing, p. 84 (in Chinese).
Zou, C., Zhu, R., Liu, K., et al., 2012. Tight gas sandstone reservoirs in China: characteristics and recognition criteria. J. Petrol. Sci. Eng. 88, 82–91. https://doi.org/10.1016/j.petrol.2012.02.001.